CrossMark

ORIGINAL PAPER

Transition from collision to subduction in Western Greece: the Katouna–Stamna active fault system and regional kinematics

E. Pérouse[1,2] · M. Sébrier[3,4] · R. Braucher[5] · N. Chamot-Rooke[1] · D. Bourlès[5] ·
P. Briole[1] · D. Sorel[6] · D. Dimitrov[7] · S. Arsenikos[1]

Abstract Transition from subduction to collision occurs in Western Greece and is accommodated along the downgoing plate by the Kefalonia right-lateral fault that transfers the Hellenic subduction front to the Apulian collision front. Here we present an active tectonic study of Aitolo-Akarnania (Western Greece) that highlights how such a transition is accommodated in the overriding plate. Based on new multi-scale geomorphic and tectonic observations, we performed an accurate active fault trace mapping in the region, and provide evidence for active normal and left-lateral faulting along the Katouna–Stamna Fault (KSF), a 65-km-long NNW-striking fault system connecting the Amvrakikos Gulf to the Patras Gulf. We further show that the Cenozoic Hellenide thrusts located west of the KSF are no longer active, either in field observation or in GPS data, leading us to propose that the KSF forms the northeastern boundary of a rigid Ionian Islands-Akarnania Block (IAB). Cosmic ray exposure measurements of ^{10}Be and ^{36}Cl were performed on a Quaternary alluvial fan offset along the KSF (~50 m left-lateral offset). A maximum abandonment age of ~12–14 ka for the alluvial fan surface can be determined, giving an estimated KSF minimum geological left-lateral slip rate of ~4 mm year^{-1}, in agreement with high GPS slip rates (~10 mm year^{-1}). Despite this high slip rate, the KSF is characterized by subdued morphological evidence of tectonic activity, a gypsum-breccia bedrock and a low level of seismicity, suggesting a dominantly creeping behavior for this fault. Finally, we discuss how the IAB appears to have been progressively individualized during the Pleistocene (younger than ~1.5 Ma).

✉ E. Pérouse
eugenie.perouse@gmail.com

1 Laboratoire de Géologie, UMR CNRS 8538, PSL Research University, Ecole normale supérieure, 24 rue Lhomond, 75005 Paris, France

2 Present Address: Division of Geological and Planetary Sciences, California Institute of Technology, Pasadena, CA, USA

3 Institut des Sciences de la Terre de Paris, UMR 7193, Université Paris VI Pierre et Marie Curie, 75252 Paris Cedex 05, France

4 UMR 7193, CNRS, UPMC, case 129, 75252 Paris Cedex 05, France

5 Aix-Marseille Université, CNRS-IRD-Collège de France, UM 34 CEREGE, Technopôle de l'Arbois, BP80, 13545 Aix-en-Provence, France

6 Saint Jayet, 36190 Orsennes, France

7 Department of Geodesy, National Institute of Geophysics, Geodesy and Geography, Bulgarian Academy of Sciences, Acad. G. Bonchev str, bl. 3, 1113 Sofia, Bulgaria

Introduction

The lateral transition from oceanic subduction to continental collision induces deformation in the overriding plate. Western Greece offers the opportunity to investigate the tectonic implications of such a transition. The old Mesozoic Ionian oceanic lithosphere (Catalano et al. 2001; Speranza et al. 2012) subducts below the Peloponnesus, while to the north, the nearby thick Apulian carbonate platform, on the same Ionian-Apulian micro-plate (D'Agostino et al.

2008; Perouse et al. 2012), abuts against the NW Greece–Albania foreland fold and thrust belt (Fig. 1). The highly seismic right-lateral Kefalonia transform fault (Figs. 1, 2), connecting the collision and subduction fronts, has been extensively studied (e.g., Louvari et al. 1999; Pearce et al. 2012). Farther east inland, NNW-striking Hellenide units and Neogene fold and thrust system (Clews 1989; Underhill 1989) are overprinted by active E–W-striking rifting systems (Gulf of Amvrakikos, Trichonis Lake, Gulf of Corinth and Gulf of Patras, Fig. 3). This distributed extension within the upper plate is possibly related to the Hellenic slab retreat (Jolivet et al. 2010; Perouse et al. 2012; Durand et al. 2014). Among the presently active rifting systems, the Corinth Rift is the one which timing evolution is the best constrained. The earliest stage of extension, distributed over a broad rift system, would have started in Pliocene (oldest syn-rift volcanic deposits are 3.6–4 Ma old, Collier and Dart 1991). The deepening of the rift and the deposition of giant fan deltas, which marks the inception of major tectonic activity in the Corinth rift is dated to ~1.7 Ma, according to the oldest syn-rift deposits age (Rohais et al. 2007a, b). Then, fault activity progressively migrated northward from 1.5 to 0.7 ka, leading to the most recent rifting phase of the Gulf of Corinth (0.7 Ma to present day) where extension is localized on the northward

dipping normal faults of the present-day southern Gulf of Corinth (e.g., Jolivet et al. 2010; Ford et al. 2013).

Previous tectonic studies of the Aitolo-Akarnania region (Western Greece) propose an active fault network consisting of a set of Quaternary E–W-striking grabens (Amvrakikos Gulf, Trichonis Lake and Patras Gulf, Fig. 3) connected by a NW-striking left-lateral fault zone (Melis and Burton 1988; Clews 1989; Sorel 1989; Underhill 1989). Active left-lateral transtension along this fault system, referred as the Amvrakia or Katouna fault, has been proposed based on local tomography (Haslinger et al. 1999), GPS data (Le Pichon et al. 1995; Cocard et al. 1999; Hollenstein et al. 2008; Vassilakis et al. 2011; Chousianitis et al. 2015) and estimated as ~11 mm year^{-1} (GPS slip rate, Vassilakis et al. 2011). However, no clear geological or morphological evidence for active left-lateral faulting has yet been provided: Studies were mainly focused on Cenozoic tectonics of the ~N-striking Hellenide fold and thrust system in Akarnania (Clews 1989; Underhill 1989), and geological evidence for left-lateral displacement was only observed within Mesozoic limestones (Vassilakis et al. 2006, 2011). The existence of a block in Akarnania bounded to the west by the Kefalonia fault, to the north by the Amvrakikos graben and to the east by a NW-striking left-lateral system joining southward to the Patras-Corinth

Fig. 1 Geodynamic setting of Western Greece. Tectonic structures and crust nature are from Chamot-Rooke et al. (2005) and Papanikolaou et al. (2006). Velocity vectors, relative to fixed Eurasia, are from the regional interpolated velocity field (Perouse et al. 2012). AP: Apulian Platform; CR: Corinth Rift; CSZ: Calabrian Subduction Zone; KF: Kefalonia Fault; NAF: North Anatolian Fault; Pel: Peloponnesus. *Black structures* are active, gray ones are inactive (cf. Perouse et al. 2012). The *blue star* is the rotation pole of the Apulian-Ionian microplate relative to the Nubian plate, shown with its 95 % confidence ellipse (Perouse et al. 2012)
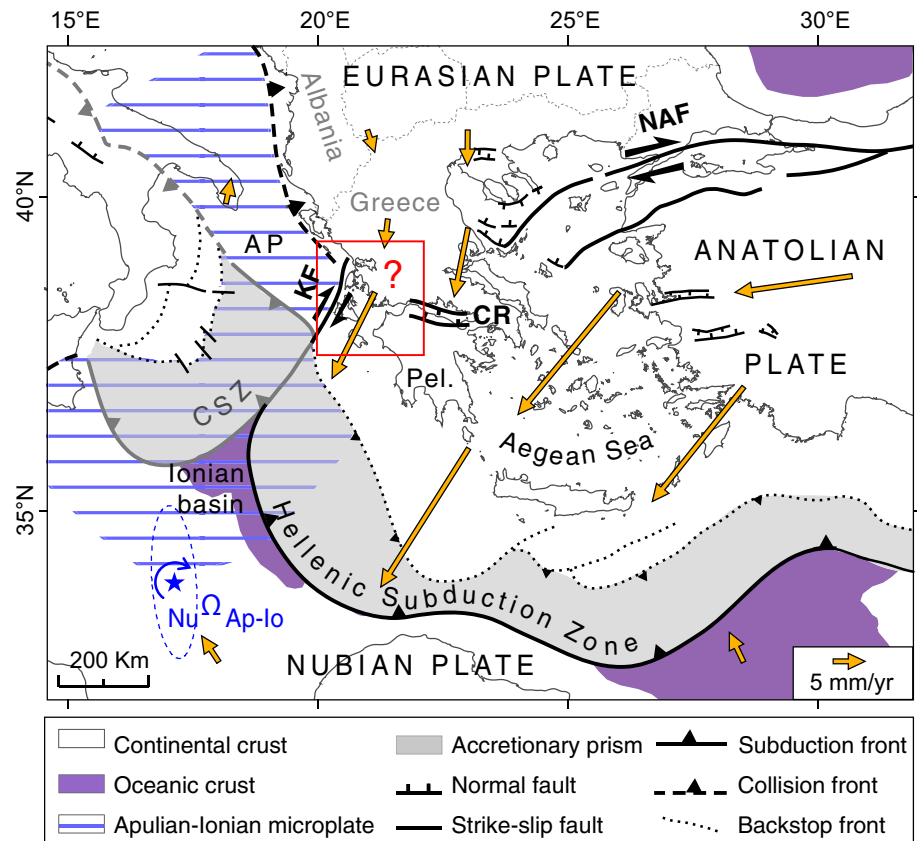
Fig. 2 Instrumental seismicity in the Western Greece region. Focal mechanisms of superficial events (<30 km) from the Harvard CMT catalog (1976–2007) and the Regional CMT catalog (1995–2007) have been relocalized according to the Engdahl catalog (Engdahl et al. 1998). Compressional quadrants of focal mechanisms: *blue*, *red* and *green* indicate reverse, strike–slip, and normal faulting, respectively. Seismicity distribution of superficial events (<30 km), with magnitude Ml > 3.7, is plotted in yellow (from NOA catalog, 1970–2008)
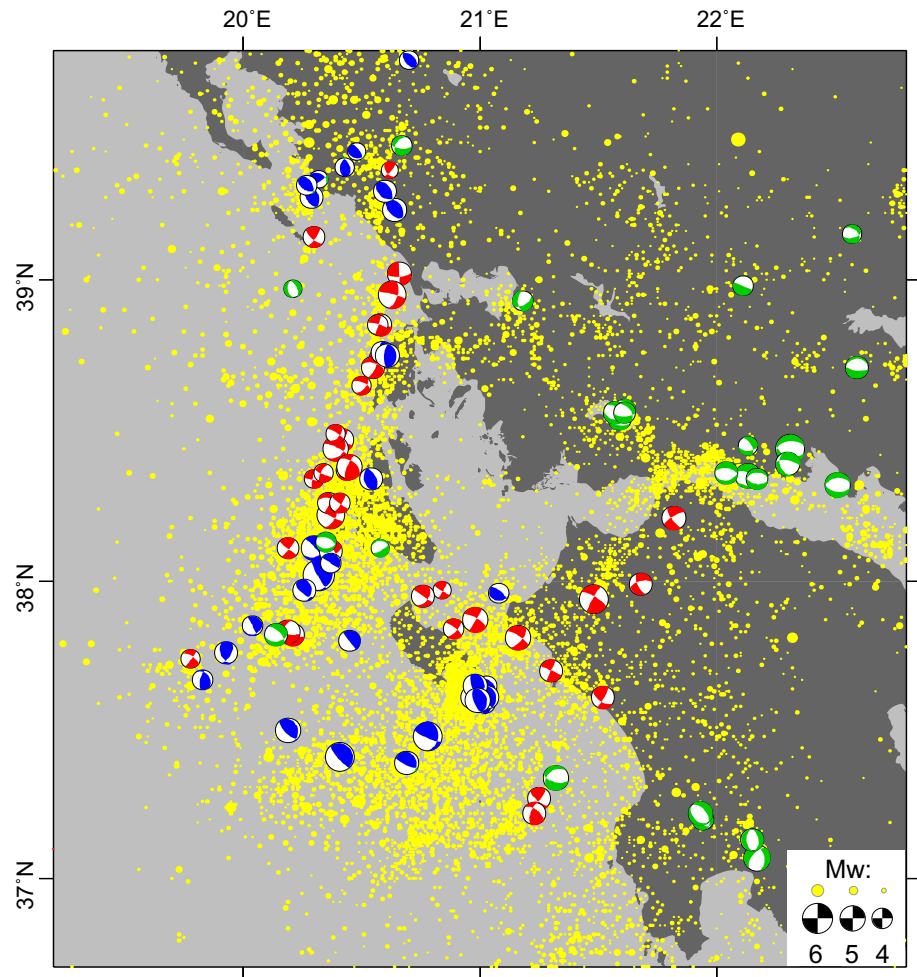
rift has been suggested (Le Pichon et al. 1995; Cocard et al. 1999; Hollenstein et al. 2008; Konstantinou et al. 2009). In the most detailed model, Vassilakis et al. (2011) proposed that the extension at the western end of the Corinth rift is transferred to the Amvrakikos graben through the Trichonis Lake graben and a left-lateral fault in the Amphilochia valley, defining the northeastern boundary of an "Akarnania fragment." Post-Pliocene out-of-sequence reactivation of the N-striking Neogene Hellenide thrusts in Akarnania (Clews 1989) as well as present-day normal faulting (Vassilakis et al. 2006) point to possible active internal deformation within this block.

The aims of our study are to accurately define the NNW-striking fault system of Aitolo-Akarnania, here informally termed the Katouna–Stamna Fault (KSF), and determine whether internal deformation occurs within the Akarnania block, along the N-striking Akarnania thrusts. Based on the analysis of satellite images, Digital Elevation Model and field studies, we performed a critical reappraisal of published data, conducted an accurate mapping of active fault traces in the region, and collected multi-scale geomorphologic observations that provide

evidence for active normal and strike–slip faulting, especially left-lateral displacement along the KSF. We further estimated a minimum geological slip rate for the KSF measuring ^{10}Be and ^{36}Cl cosmogenic radionuclides produced in situ. Our new results on the active tectonics of Akarnania are discussed in the light of existing and new GPS data.

Morphotectonic study of Aitolo-Akarnania

Figure 3 is a map summarizing active and inactive major structures of Western Greece from our reappraisal of the tectonics of the Akarnania region. In our study, we consider faults to be "active" if they control the landscape morphology at first order (offset streams, structural landscape, upward convex-shaped profile, etc.) and/or if they offset Quaternary deposits. By opposition, faults are considered to be "inactive" when the landscape morphology results mainly from erosional processes. Our contributions to Fig. 3 map concern the Katouna–Stamna Fault (KSF, Fig. 4), its northward termination onto the Loutraki

Fig. 3 Tectonic map of Western Greece showing active (*red*) and inactive (*black*) faults. Lou: Loutraki fault; Tri: Trichonis Lake. Fault traces from the present study: Loutraki and KSF. Fault traces from other studies: onshore Ionian islands (Cushing 1985; Nielsen 2003); offshore Amvrakikos (Anastasakis et al. 2007); Trichonis graben (Perouse 2013); Patras Gulf (Ferentinos et al. 1985); Corinth Rift (Jolivet et al. 2010); Apulian collision front, Hellenic backstop, Calabrian prism (Chamot-Rooke et al. 2005); Achaia-Elia fault (e.g., Stiros et al. 2013), N-striking Akarnania thrusts (Clews 1989, see Fig. 4 for details). Hellenides units: *yellow*, Pre-Apulian zone (PA zone), *purple*, Ionian zone, *brown*, Gavrovo-Tripolitza (Gvo-Tz) and *green*, Pindos unit (Aubouin 1959; British Petroleum Co Ltd 1971; Karakitsios and Rigakis 2007). Neogene and Quaternary deposits in white. *Inset* regions names. Aka: Akarnania; Aito: Aitolia; Pelop: Peloponnesus
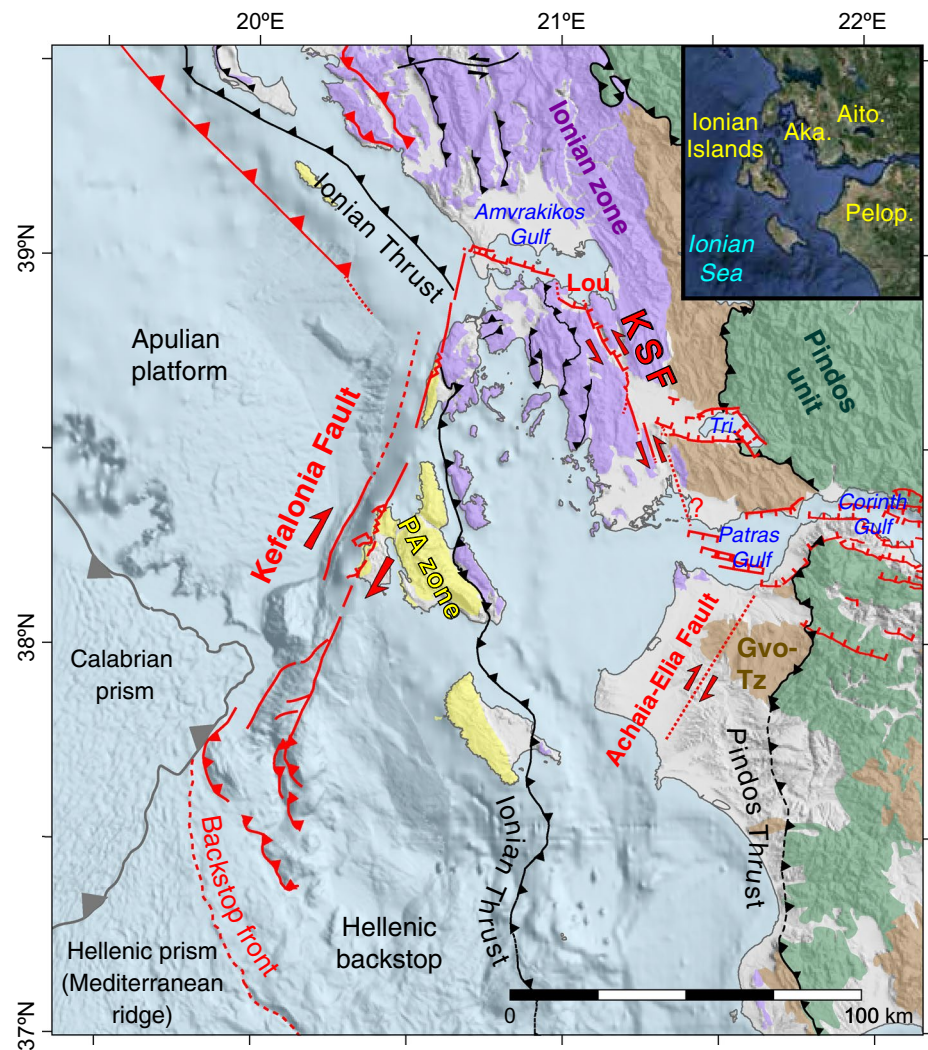
fault, and a reappraisal of the N-striking Akarnania thrusts, located west of the KSF (Figs. 3, 4).

Evidence for active vertical slip component along the northern KSF (Loutraki fault and Katouna valley fault)

One prominent geomorphic feature in Akarnania is the remnant of a large uplifted paleo-surface on Triassic breccias, tilted ~4° southward, ~700 m high, south of the Amvrakikos Gulf nearby the Katouna valley (Figs. 4, 5). This paleo-surface ends abruptly northward where it is cut by the ESE-striking Loutraki fault. This fault shows the typical morphology of an active normal fault escarpment: overall upward convex-shaped profile (Wallace 1978), wineglass valleys, and triangular facets (Figs. 5, 6). The ~4° southward tilt of the paleo-surface is highlighted by a reverse sense of drainage in the windgap shown on Fig. 5a. The overall morphology can be simply interpreted as the result of footwall uplift and southward tilt associated with the northward dipping Loutraki normal fault. Topographic

profiles crossing the Loutraki fault escarpment (profiles L1, L2 and L3 in Fig. 6) show two benches that represent either several parallel migrating faults (i.e., "paleo" scarps) or interaction between footwall uplift and notching due to headward erosion from high stand sea levels. In either case, the location of the present-day active normal fault would be at the base of the escarpment (Figs. 5, 6). It would account for the topography (footwall uplift southward of the fault/hanging-wall subsidence northward of the fault) and the occurrence of incision southward of the fault, compatible with footwall uplift (Fig. 5). A more complex fault geometry occurs east of the Loutraki Fault. Here, we observed in the field (1) a normal F1 fault plane between Mesozoic limestones and old alluvial fan deposits (N120° 55°N 85°E, FP on Fig. 5); (2) incision to the north of F1 within old alluvial fan deposits. This incised alluvial fan is bounded to the north by an E-striking slope break. We interpret this slope break as resulting from an additional normal fault (F2 on L1 profile of Fig. 6), which controls the uplift of the old alluvial fan deposits and the subsidence in the Amvrakikos
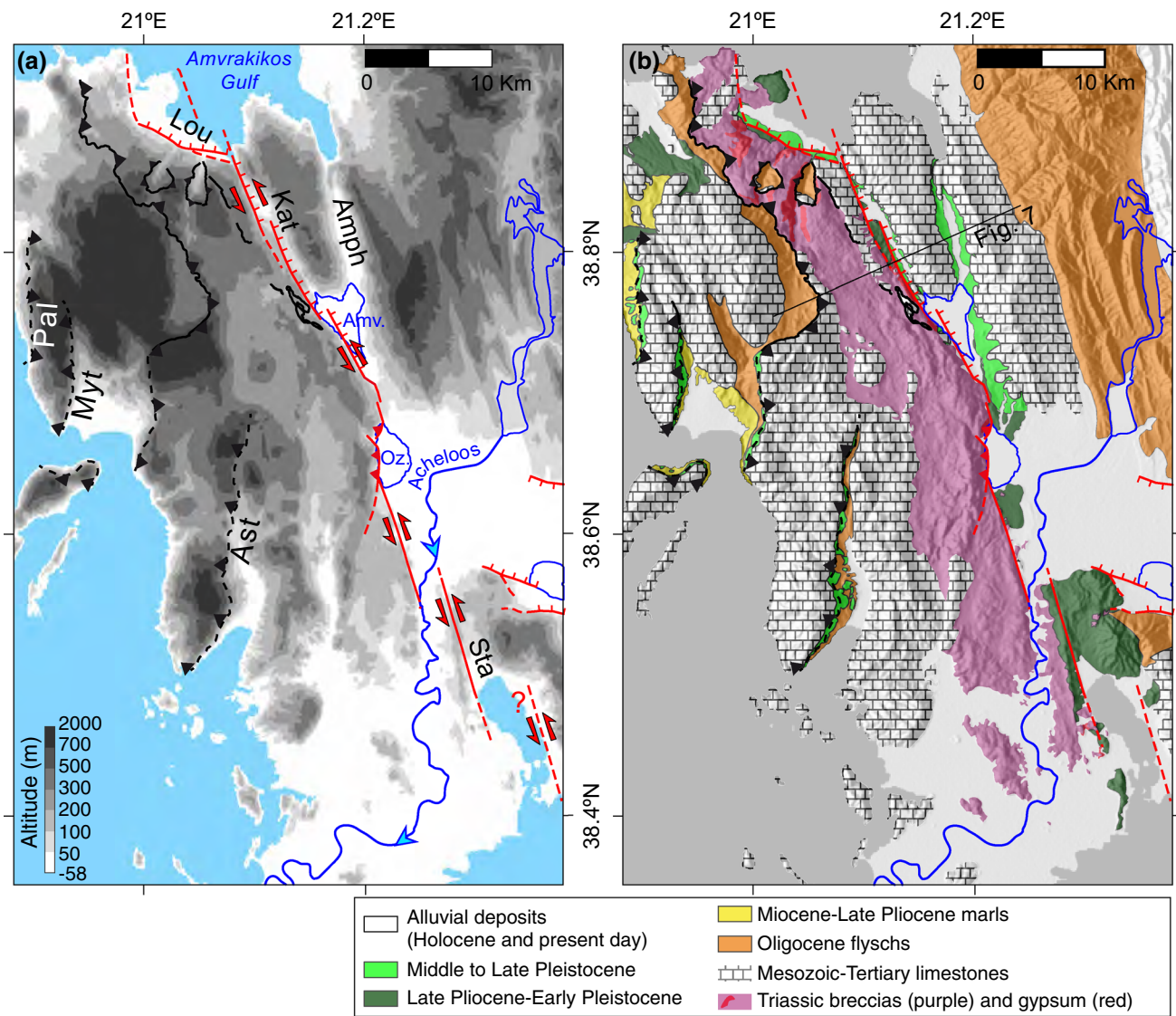
Fig. 4 Map of the KSF system. Active (*red*) and inactive (*black*) fault traces. Lou: Loutraki Fault; Kat: Katouna Fault; Sta: Stamna Fault; Amph: Amphilochia valley; Amv: Amvrakia Lake; Oz: Ozeros Lake. The Neogene Hellenides Akarnania thrusts are shown as Pal: Paleros thrust; Myt: Mytikas thrust; Ast: Astakos thrust. **a** Topography back-ground, SRTM (3s resolution); **b** Simplified geological map based on our reappraisal and geological maps (British Petroleum Co Ltd 1971; Institute of Geology and Mineral Exploration IGME 1987). Sealed thrusts are shown with *dashed lines*

Gulf. Thus, to the east of the Loutraki Fault, deformation could have migrated northward onto a younger fault segment F2, owing to the growing depression caused by rifting in the Amvrakikos Gulf.

South of the Loutraki fault, the uplifted paleo-surface is bounded to the east by pronounced N158°- to N152°-striking, E-facing linear slopes with upward convex profiles (Figs. 5a, 6), such kind of escarpments are typically associated with normal fault in the US Basin and Range province (Wallace 1978). These linear E-facing escarpments are carved within easily erodible gypsum along the Katouna valley. The preservation of such escarpments in

gypsum demonstrates that faults have a high level of activity. In addition, the fairly planar geometry of these escarpments indicates they correspond to the exhumation of normal fault plans. Moreover, the British Petroleum Co Ltd (1971) mapped an east-dipping normal fault in the Katouna valley. According to our geological cross section (Fig. 7), a fault with a vertical slip component is actually necessary in the Katouna valley to account for the anomalous contact between Triassic gypsum and Early Cretaceous limestones. Our cross section also intersects the southern termination of a northern segment (Fig. 5). Upper Pliocene-Early Pleistocene lacustrine deposits are uplifted along one of these

Fig. 5 **a** Morphological map of Loutraki and Katouna Faults. Topography background with height contours, SRTM (3s resolution). Main drainage network is in *blue*. *Solid round-shaped black lines* wine glass valleys; *dashed black line* benches on Loutraki fault escarpment. **b** Simplified geological background (same captions as Fig. 4b). The FP yellow point is a normal fault plane N120° 55°N 85°E, between Mesozoic limestones and old alluvial fan deposits (38.864572°N, 21.070004°E)
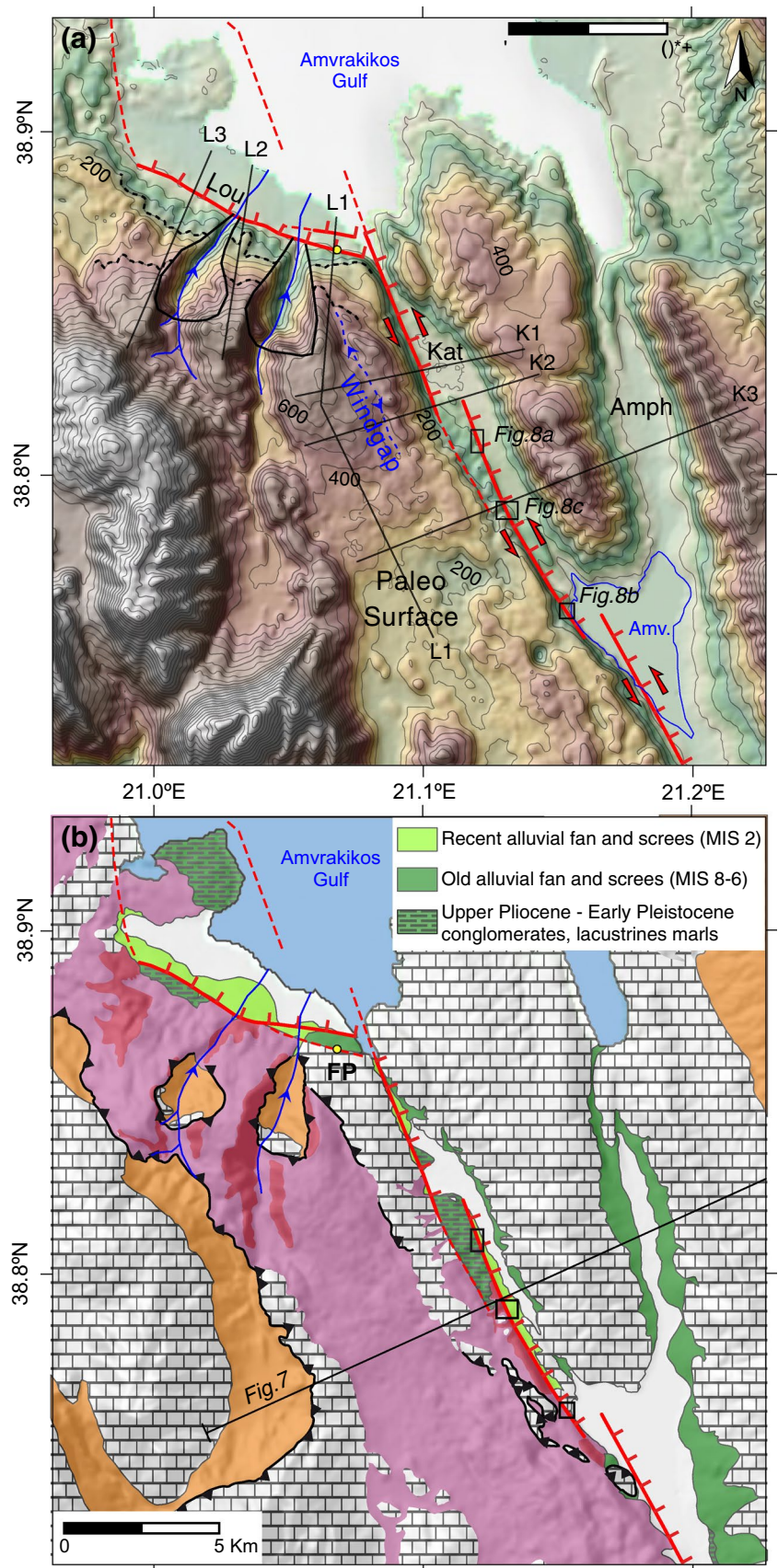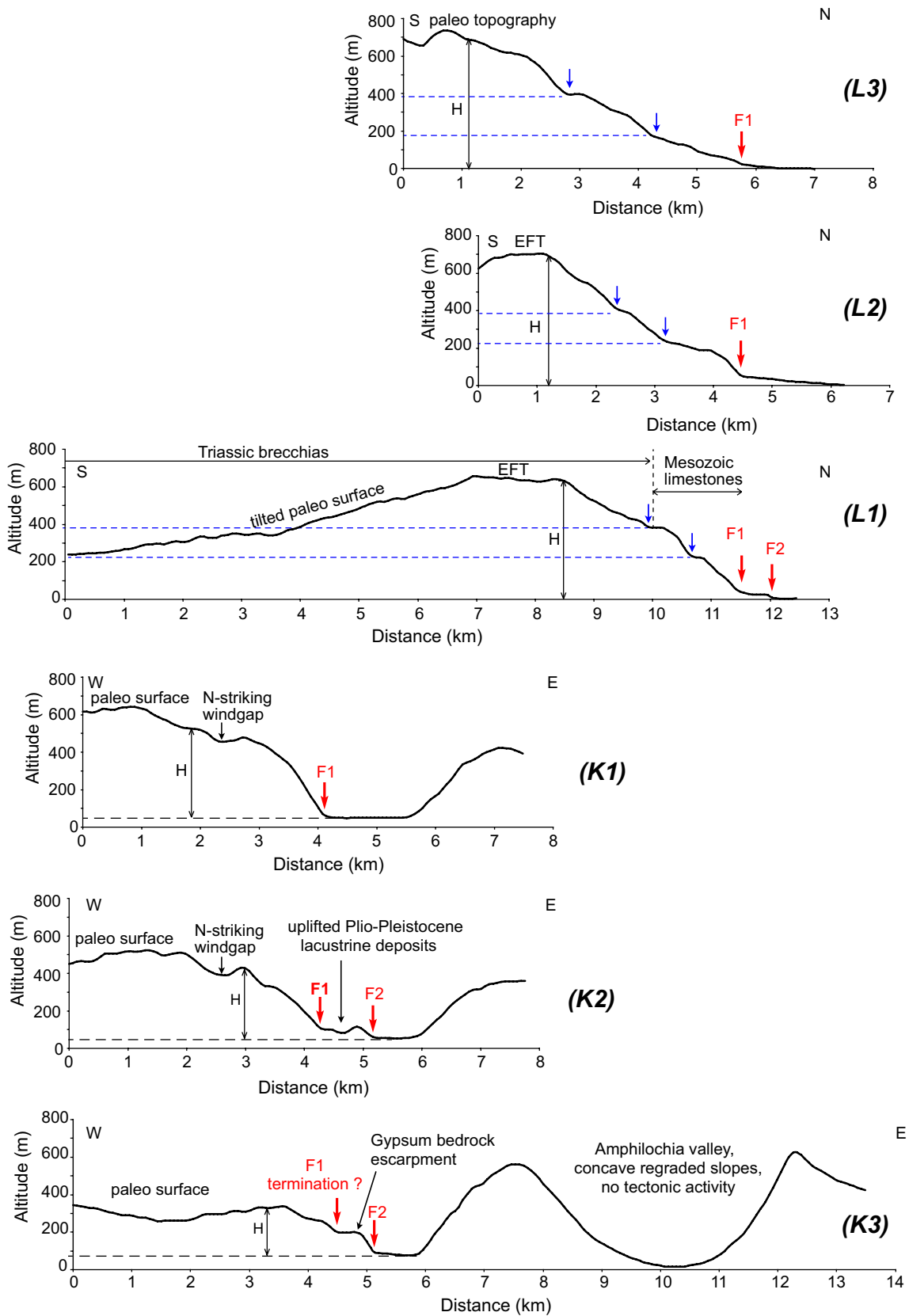
Fig. 6 Topographic profiles across the Loutraki and Katouna Faults, with vertical exaggeration (×3). Profile lines are plotted in Fig. 5. *H* escarpment height, *EFT* escarpment flat top; *blue arrows* benches; *red arrows* active faults
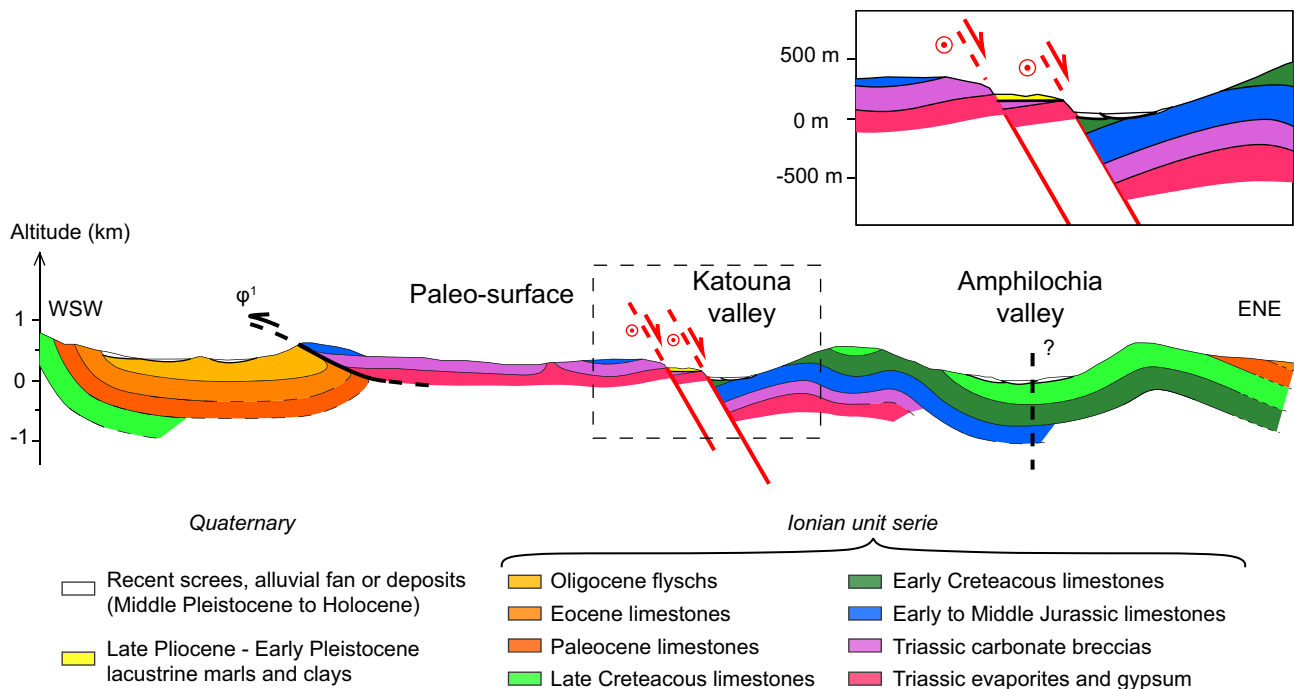
Fig. 7 Geological cross section through the Katouna and Amphilochia valley, based on the 1:50,000 Amphilochia geological map (Institute of Geology and Mineral Exploration, IGME 1987), and our interpretative Katouna fault geometry. Section line is plotted in Figs. 4, 5

faults (profile K2 on Fig. 6, yellow formation on Fig. 7). The inferred total vertical throw across the fault segments reaches 750 m (~300 m of footwall uplift, ~450 m of hanging-wall subsidence). The steep dip proposed in our cross section follows the linear fault traces at the surface (Fig. 5). A steep east-dipping normal fault agrees with the occurrence of micro-seismicity at 20 km depth, slightly east of the Katouna valley (Hatzfeld et al. 1995). We thus interpret the Katouna valley as a structural landscape, the morphology being controlled by active steep eastward dipping normal fault segments.

Comparing the Katouna valley with the nearby Amphilochia valley to the east suggests this major valley is quite different (Fig. 5). Previous studies (Vassilakis et al. 2011) and geological maps (British Petroleum Co Ltd, 1971; Institute of Geology and Mineral Exploration, IGME 1987) have proposed this valley to be an active left-lateral strike–slip fault zone. First of all, along the Amphilochia valley, the topography follows directly the geological folding (i.e., the valley bottom coincides with a syncline axis, Fig. 7), suggesting that a large part of this depression could be inherited from Tertiary folding. The vertical throw of the hypothetic fault is small as the same layer is cropping out on both side of the reported fault (Fig. 7), and the concave regraded slopes of the valley (profile K3, Fig. 6) do not suggest any active vertical component for the fault (Wallace 1978). This could be compatible with a pure

strike–slip fault running in the middle of the valley bottom (as suggested by the geological map of the Institute of Geology and Mineral Exploration, IGME 1987), and covered by constantly aggrading Holocene deposits. However, the lack of benches and elongated small depressions along the possible fault trace within the hard limestones on the northern Amphilochia valley do not agree with any active strike–slip fault along the Amphilochia valley. Therefore, we propose that most of the northern KSF deformation is presently accommodated along the Katouna valley.

Evidence for active left-lateral motion along the KSF

In the previous section, we show that the total escarpment height of the Loutraki normal fault is ~700 m (Fig. 6). As the KSF, eastern border of the uplifted paleo-surface, is linked to the Loutraki fault in its northern termination, the KSF escarpment height is directly controlled by the Loutraki escapement height in its northernmost section. However, far enough from the Loutraki fault, at the west of the Amvrakia lake, the altitude of the uplifted paleo-surface becomes stationary at about ~300 m high (Fig. 5), suggesting that this area is no longer influenced by the Loutraki footwall uplift and tilt (Figs. 5, 6). Then, in this area, the uplifted paleo-surface would be only due to the KSF footwall uplift (~300 m). The conspicuous difference in footwall uplift (with 2 to 1 ratio) between the Loutraki normal

fault and the Katouna valley faults indicates that either the Loutraki fault initiated earlier or the Katouna valley faults are not purely normal. The second option is more likely because the KSF fault segments show a typical en-echelon pattern with left stepovers systematically associated with depressions (Katouna valley, Amvrakia lake, southern Acheloos river valley, Aitoliko lagoon, Fig. 4). Along the KSF, only one right stepover occurs, and it is associated with a range in easily erodible Triassic breccias and gypsum, at the western border of the Ozeros lake (oz. on Fig. 4). These observations are thus compatible with left-releasing stepovers and right-restraining stepover, respectively, implying a left-lateral component along the KSF fault segments. At the right-restraining stepover location (oz. on Fig. 4), we surmise a possible low-dip east-verging thrust to account for the range west of the Ozeros lake depression (flexural depression due to a possible east-verging thrust). Accounting for this oblique-slip and aware of the difficulty to connect the same objects across this type of fault, we concentrate our observations on local drainage crossing the KSF to retrieve evidence for left-lateral offsets. As it may be expected on an oblique-slipping fault, we did not find any conspicuous dogleg offset. Nevertheless, we identified several potential offsets along the southern fault segment of the Katouna valley where 8 streams are left-laterally diverted with finite displacements ranging from 5 to 50 m (five of these stream offsets are shown on Fig. 8). One could argue that such stream diversions may result from the random meanderings of the downstream channels on top of the young alluvial fans located in the hanging-wall block. However, small diverted streams are observed on the northern termination of the southern fault segment of the Katouna valley, where the fault displacement and escarpment disappear (Fig. 8a). Here the stream channels incise in similar alluvial material on both sides of the KSF. Thus, these small diverted streams are more likely to preserve true left-lateral fault displacements (Fig. 8a). Interestingly, they appear to record some ~ 10 m of left-lateral offset while larger streams display higher amounts of left-lateral offset, the maximum value being ~50 m (Fig. 8c). It must be stressed that, as has been reported for the San Andreas Fault, many streams do not display any offset or can even show right-lateral diversions (e.g., Gaudemer et al. 1989).

We also found some evidence of active strike–slip motion in the Stamna area, to the south of the Katouna valley (Sta on Fig. 4a). Here, a N162°-striking linear depression extends ~5.5 km from the southwesternmost tip of the Trichonis depression to the Stamna village (Fig. 9). This linear depression is carved within Plio-Pleistocene deposits, close to the limit with Triassic breccias (Fig. 4b), forming a 300- to 400-m-wide, ~10-m-deep, flat-bottomed, perched valley, with similar heights of both western and eastern valley divides (Fig. 9). This perched valley is drained by small streams only and thus appears oversized (Fig. 10). This peculiar feature is interpreted as due to the differential erosion of the sheared zone along an active N162°-striking strike–slip fault. This would account for the dominant linear drainage network (Fig. 10) and the small streams flowing nearly orthogonally toward the perched valley, whereas the major natural draining outlet of the area is the Aitoliko lagoon (Figs. 9, 10). This suggests these small streams result from headward erosion associated with the tectonically controlled perched valley. Interestingly, a small fault plane (N162° 65°W 13°S, Fig. 11) within Plio-Pleistocene deposits has been observed along the perched valley. The absence of morphological evidence for active vertical component (i.e., no fault escarpment and same height for perched valley divides), as well as the sub-horizontal slickensides of the fault plane (Fig. 11), suggests a nearly pure strike–slip faulting along the Stamna segment. Unfortunately, drainage network does not allow characterizing the sense of slip along the Stamna segment (i.e., no clear left-lateral offset stream, Fig. 10). We can only propose a left-lateral slip for the Stamna segment based on the overall KSF segments geometry (i.e., left-releasing step overs north and south of the Stamna segment, Fig. 9). Moreover, the left-lateral slip indicated by the slickensides on the observed fault plane also agrees with left-lateral motion (Fig. 11).

Overall, the KSF thus depicts a 65-km-long NNW-striking active fault system extending from the Patras Gulf to the Amvrakikos Gulf (Figs. 3, 4). KSF segments are typically ~10 km-long. Motion along the KSF evolves from left-lateral transtension on faults segments striking N158°–N152° (Katouna area) to nearly pure left-lateral strike–slip on segments striking N162° (Stamna area).

Internal deformation within Akarnania? Investigating the N-striking Akarnania thrusts

External Hellenides orogen in Akarnania led to the formation of both W- and E-verging, N-striking thrusts during the Neogene (Clews 1989; Underhill 1989). These N-striking thrusts are located to the west of the present KSF and separate Mesozoic limestones in the hanging-walls from Tertiary molasses and flysch basins in the footwalls (Paleros, Mytikas, and Astakos thrusts, Fig. 4). Post-Pliocene out-of-sequence reactivation of these thrusts have been proposed (Clews 1989), as well as present-day normal faulting along the Astakos thrust (Vassilakis et al. 2006). However, we report below some geologic, tectonic, and geomorphic observations suggesting these Cenozoic thrusts are no longer active.

The contact between Ionian Mesozoic limestones thrusting eastward over Oligocene flysch deposits is exposed to the south of the Astakos fault (Fig. 12a). Nevertheless,

Fig. 8 Offset streams along the southern Katouna fault. Sites locations are plotted on Fig. 5. Site **a** displays three stream offsets. The field photograph and the enlarged inset show a close-up of two small stream offsets of 5–7 m and ~12 m, respectively. Site **b** displays a ~40 m offset stream. Site **c** is an offset stream with a 54 ± 4 m offset. Satellite images from Google Earth
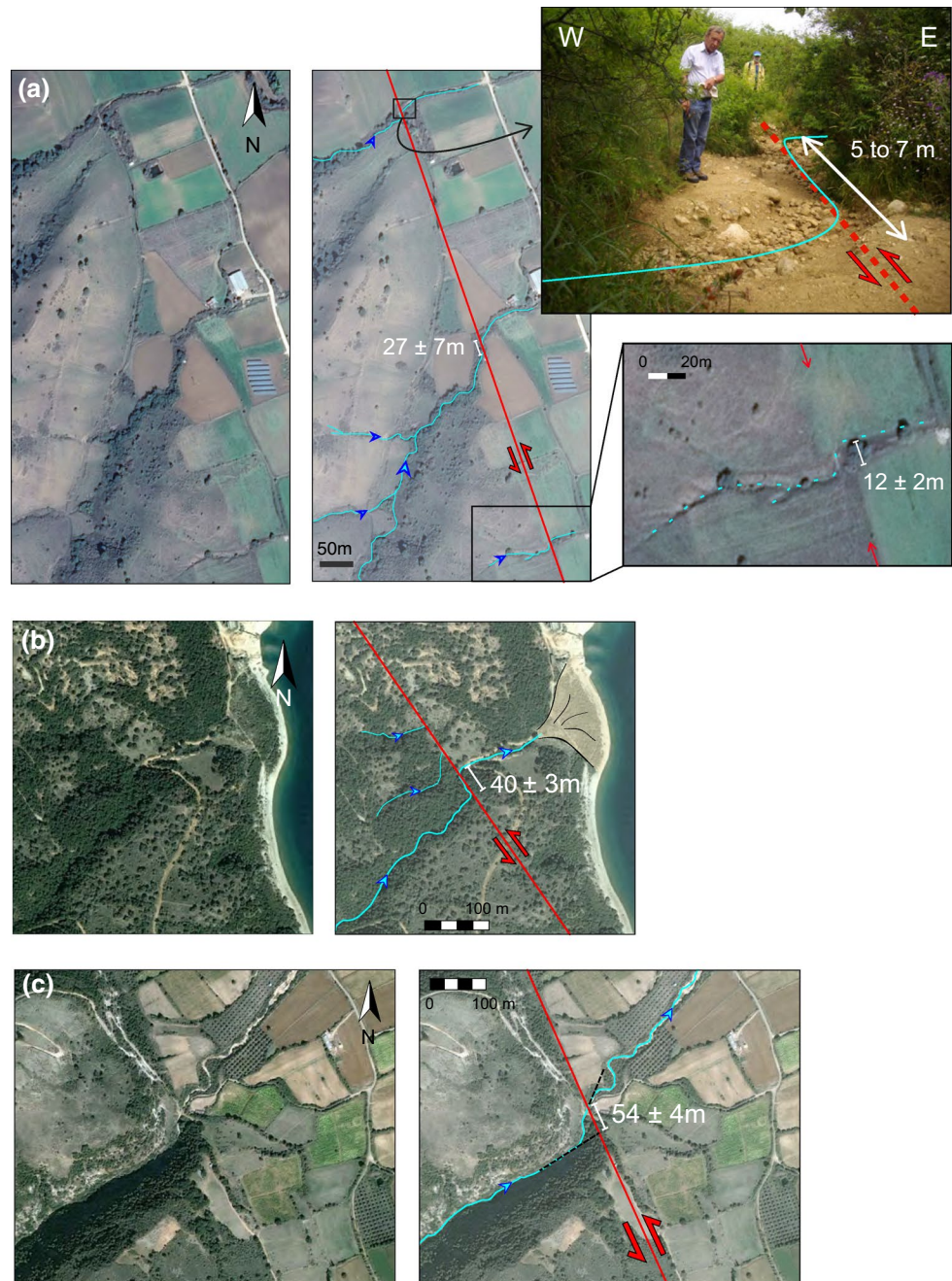
this E-verging thrust is seen sealed by strongly calcite-cemented breccias (SBr. on Fig. 12a). These breccias consist of cryoclastic angular elements with no clay matrix, which result from limestone bedrock degradation during a cold climate. Such kind of strongly calcite-cemented breccias are attributed to the Middle Pleistocene (~600 ka, Sorel 1976). The fault sealing indicates that no tectonic activity has occurred along the Astakos thrust for the last ~600 ka. Farther north, along this Astakos thrust, destroyed houses of the Paleo Karaiskakis village stand on the Oligocene flysch deposits. At this place, a roughly N-striking,

curved scarp points to the limit between the Ionian limestones and their screes, overlying the flysch deposits and hiding the Astakos thrust contact (Fig. 12b). We interpret this curved scarp trace as a landslide head scar, caused by gravitational processes that occurred within the flysch deposits and destroyed the Paleo Karaiskakis village. The N-striking normal fault reported close to Astakos village (Vassilakis et al. 2011) should correspond to similar gravitational processes. Therefore, in the Astakos area, there is no evidence for tectonic activity either on the Astakos thrust or on N-striking normal faults.

Fig. 9 a SRTM (3s resolution) of Stamna area and **b** interpreted Stamna active fault segment
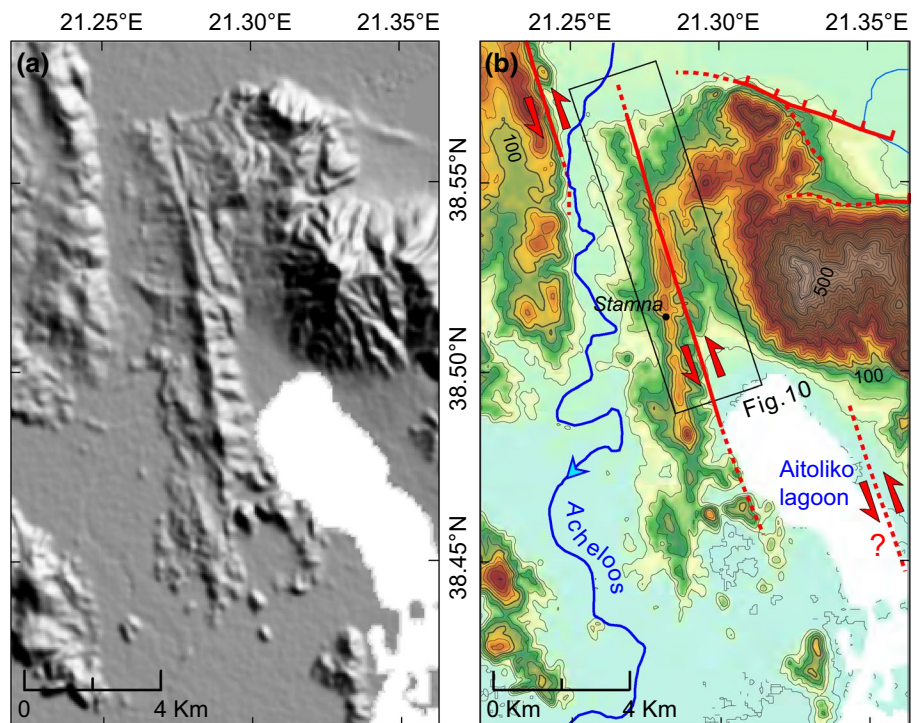
Strongly cemented slope breccias are also observed sealing the W-verging Paleros thrust front (Fig. 12c). At some places, a discontinuous linear cliff highlights the contact between the Ionian Mesozoic limestones, covered by strongly cemented breccias, and the more erodible Miocene molasses deposits. This linear feature could be interpreted as an active normal fault scarp. However, the along-strike strong variation of cliff height (red arrows on Fig. 12c) results more likely from differential erosion between Miocene sandy molasses and the limestone rocks (Ionian Mesozoic and Quaternary slope breccias). This observation also agrees with a lack of tectonic activity along the Paleros thrust. Similar conclusions can be derived from observations along the Mytikas E-verging thrust.

All our geomorphic/tectonic observations in central Akarnania are summarized in a conceptual sketch (Fig. 13). They show the N-striking Akarnania thrusts presently inactive, and some apparently normal fault scarp resulting from gravitational processes and/or gully differential erosion. As there is no evidence for significant active deformation in Akarnania west of the KSF, we consider Akarnania as a rigid block.

Cosmic Ray Exposure (CRE) dating of an offset alluvial fan along the KSF and minimum geological slip rate

Along the Katouna valley, the normal component of slip of the KSF cannot be constrained because the hanging-wall displays recent alluvial or colluvial deposits that are not present in the footwall block. In contrast, the horizontal component of slip may be estimated thanks to diverted streams that appear to record the left-lateral component of the KSF (See previous section). Two small streams show convincing offsets of ~10 m (Fig. 8a). We are not aware of any data that could provide an age estimate of these streams. They could correspond to the mid-Holocene incision (5–7 ka), which is subsequent to the sapropel sedimentation in the Mediterranean domain (Gasse et al. 2015). Such an assumption would lead to a maximum slip rate of ~2 mm/a. However, these small incisions might also correspond to younger climatic episodes, or even to historical ones. Hence, they cannot be used to derive accurate slip rates. Thus, we focused on the largest stream offsets as they may provide, due to their deeper incisions within the proximal part of the younger alluvial fans, more favorable conditions for radiometric dating.

Description and location of the sampling site

The site selected to perform cosmic ray exposure (CRE) dating is the largest left-laterally offset stream where the upslope part of a displaced alluvial fan forms a shutter ridge facing a ravine incised into the footwall escarpment of the southern Katouna fault (Fig. 14). To the east of the fault, the downstream prolongation of this ravine forms a ~6-m-incised gully in the alluvial fan (Fig. 14c). The gully is left-laterally offset by 54 ± 4 m (Fig. 14b). As alluvial
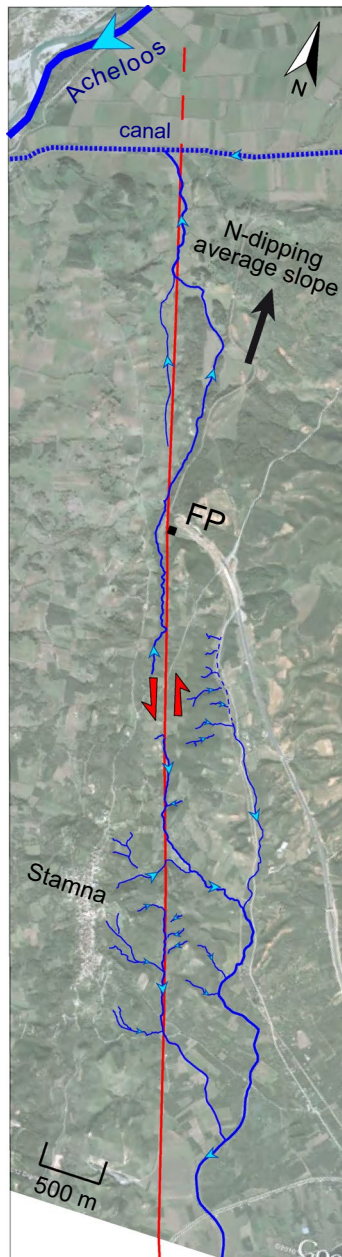
Fig. 10 Drainage network along the Stamna Fault (satellite image from Google Earth, see Fig. 9 for location). *FP* fault plane shown in Fig. 11, close to the freeway bridge

Fig. 11 Fault plane measured within Plio-Pleistocene alluvial deposits (location on Fig. 10). Fault plane is N162° 65°W, with a 13°S dipping slickenside (underline by the *red line*), indicating a nearly pure left-lateral slip

fan aggradation and abandonment predate gully incision, the age of the alluvial fan abandonment provides the upper bound age for the gully incision. Dating this abandonment using in situ-produced cosmogenic nuclides should provide an estimate of the minimum geological horizontal slip rate of the Katouna fault. The CRE dating method is widely used to constrain cosmic ray exposure duration of geomorphic features. App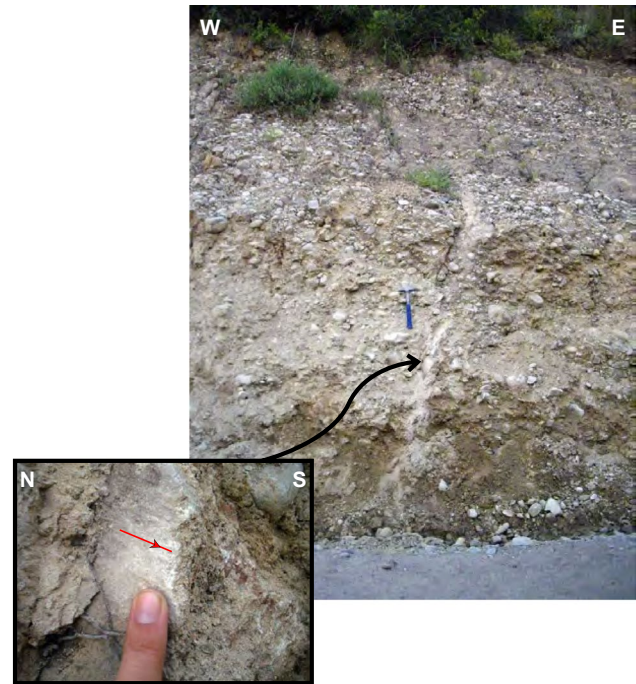lied to an alluvial fan, the CRE age reflects the abandonment age of the alluvial surface after its aggradation and before its subsequent incision.

The sampling site is a natural outcrop carved within the offset alluvial fan material, where the external part of an active meander forms an active cliff (Fig. 15). Remnants of historical-time flood deposits within the bottom of the gully incision indicate that the outcrop is frequently rejuvenated and has consequently not been long exposed. As the top of the alluvial fan is covered by ~1.20-m-thick shard bearing, historical colluvium, we sampled ~5.30-m-high depth profiles without collecting any surface sample (Fig. 15). The alluvial material crops out on a 4.10-m section and consists of proximal debris flow with subangular to subrounded elements (gravels and cobbles), comprising reworked Mesozoic limestones and flints from the Ionian unit series. Due to the nature of these elements, we sampled along two depth profiles: one including only cherts and the other only carbonates to perform concentration measurements of in situ-produced ^{10}Be and ^{36}Cl cosmogenic nuclides, respectively. Sample preparations were performed at CEREGE (Aix-en-Provence) and AMS measurements at the French national AMS facility ASTER (CEREGE, Aix-en-Provence) (detailed procedures are given in Supplementary Material).

Fig. 12 Field photographs of the N-striking Neogene thrusts in central Akarnania. Location of thrusts on Fig. 4a. **a** View of the Astakos thrust sealed by strong calcite-cemented breccias (SBr). SBr consists of cryoclastic angular elements of Ionian Mesozoic limestone with no clay matrix attributed to the Middle Pleistocene (Sorel 1976); **b** landslide head scar along the Astakos thrust. *White arrows* indicate this head scar. The destroyed house on the left attests for a recent landslide movement. *Inset* shows the scar of the last movement. PBr: poorly consolidated slope breccias. They may correlate with either Holocene or the last climatic crisis coeval with LGM (i.e., MIS 2); **c** W-facing discontinuous cliff made of Ionian Mesozoic limestone covered by strongly cemented slope breccias (SBr) seen along the Paleros thrust. This cliff height displays an along-strike variation (*red arrows*) resulting from gully differential erosion between the limestone material and the Miocene molasses
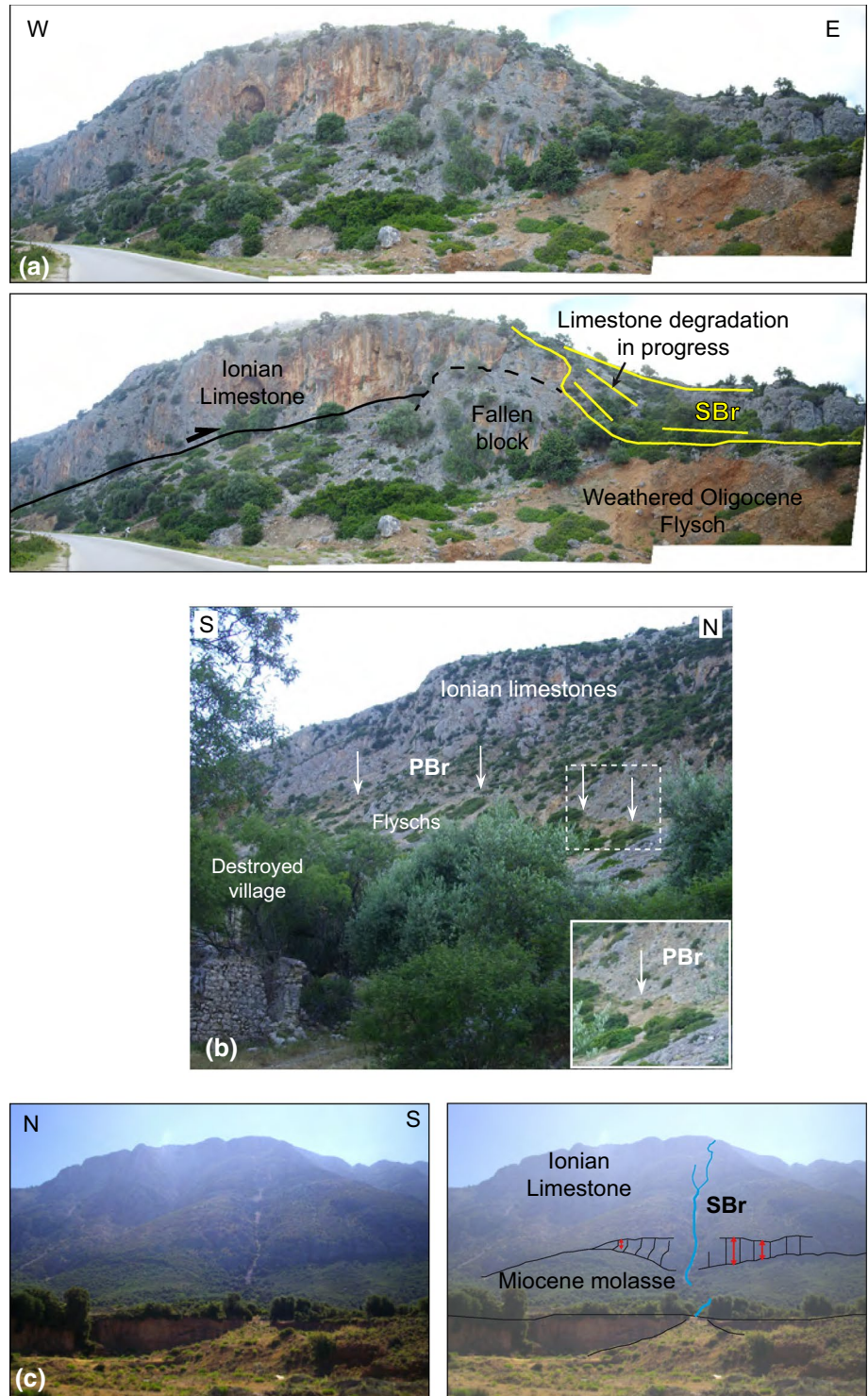
CRE dating results and minimum geological slip rate

Cosmogenic nuclide concentrations measured as a function of depth are controlled by three parameters: (1) the exposure duration to cosmic rays at the sampling depth; (2) the denudation rate affecting the sampled surface and, (3) the inherited cosmogenic nuclide concentration accumulated during a pre-exposure history and/or the transport from the source region (inheritance). In case of homogeneous inheritance, the in situ-produced cosmogenic nuclide concentrations decrease exponentially with depth and tend to an asymptotic value of zero (no inheritance) or nonzero, corresponding to the amount of the measured concentration that is inherited (Siame et al. 2004; Braucher et al.
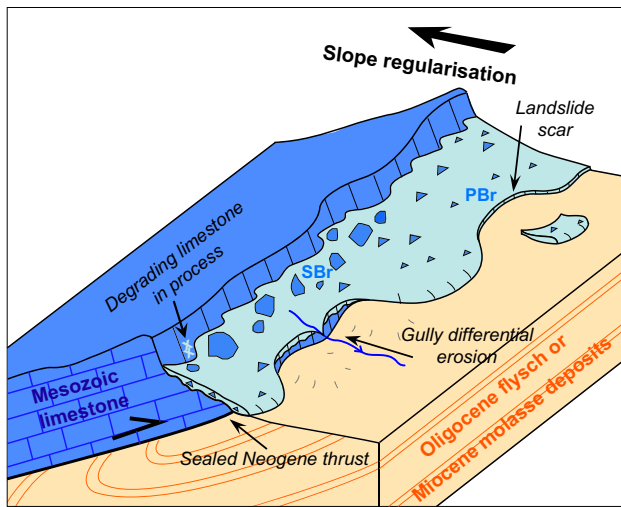
Fig. 13 Conceptual 3D block diagram summarizing tectonic and geomorphologic field observations seen on the N-striking Akarnania thrusts (Fig. 12) and interpretations

2009). In this case, the three unknown parameters can be determined from the modeling of measured depth profile concentrations.

The presented results do not show such a distribution (Fig. 16). Measured ^{10}Be and ^{36}Cl concentrations are both scattered and do not exhibit any exponential decrease with depth, indicating most likely that the samples were deposited in the alluvial fan with a highly variable inherited component. In addition, ^{36}Cl surface in situ production rate is significantly higher than ^{10}Be surface in situ production rate (Nishiizumi et al. 2007; Schimmelpfennig et al. 2009). Therefore, measured ^{36}Cl concentrations significantly lower than ^{10}Be concentrations along the profile may indicate that chert samples were exposed to cosmic ray prior to their deposition in the alluvial fan for a much longer time period than carbonate samples, leading to a more concentrated ^{10}Be inherited component in cherts than the ^{36}Cl inherited component in carbonates. On the other hand, measured in situ-produced ^{10}Be concentrations largely exceed the maximum allowed ^{10}Be concentration that corresponds to infinite exposure duration on a noneroding surface (Suppl. Material, Table S1). This then suggests a possible adsorption of ^{10}Be at the surface within amorphous silica as recently evidenced (Zerathe et al. 2013). For all these reasons, measured ^{10}Be concentrations in cherts are not suitable for dating the alluvial fan abandonment age.

Nevertheless, the ^{10}Be concentrations accumulated during an assumed infinite pre-exposure duration correspond to the steady-state ^{10}Be concentrations that only depend on the denudation rate. They give therefore the opportunity to calculate maximum denudation rates (ε_{max}) (Suppl. Material, Table S2). As source regions for cherts should be the

Ionian zone (Suppl. Material, Fig. S1), a possible explanation to account for such high inheritance would be that these cherts have been spread as residual elements onto the Katouna paleo-surface that eroded most of the Ionian thrust sheet, up to the Triassic breccias. This paleo-surface is presently eroded by the upstream catchments of the alluvial fan (Fig. 14a) allowing cherts to be transported and aggraded downstream in the alluvial fan. The maximum denudation rates (ε_{max}) determined on cherts would thus correspond to the denudation of the Katouna paleo-surface. Most of these calculated ε_{max} are lower than 5 m/Ma (Suppl. Material, Table S2), suggesting a relatively low denudation rates for the region.

The carbonate ^{36}Cl concentrations, ranging from 1.10^5 to $2.5.10^5$ at/gr. (Fig. 16) are less scattered than those of ^{10}Be. Carbonate elements, sampled in the same alluvial fan as the cherts, thus carry a less complicated pre-exposure history. Hence, it allows modeling the in situ-produced ^{36}Cl concentrations, and then to estimate an abandonment age for the alluvial fan. As the upper 1.20 m of the depth profile consists of historical colluviums, we consider that the initial fan surface is located at 1.20 m depth below the surface. Consequently, the CRE age modeling of the alluvial deposits was performed on the carbonate samples below 1.20 m depth (Fig. 17b). The scattering of the measured ^{36}Cl concentrations and the occurrence of high ^{36}Cl concentrations in the deepest part of the profile suggest variable inherited ^{36}Cl concentration in the carbonate samples, that do not permit to run a simple CRE age modeling assuming an homogeneous inheritance. In case of variable inheritance, a rejuvenation depth profile analysis (Le Dortz et al. 2012) allows providing a maximum abandonment age for the fan surface. Assuming a negligible denudation rate as estimated from the ^{10}Be concentrations (Suppl. Material, Table S2), this rejuvenation analysis provides a maximum exposure duration (i.e., abandonment age) for the alluvial fan surface of ~10 ka (Fig. 17b; Table 2). Then, the sensitivity of this abandonment age has been tested for different denudation rates of 5, 20, and 30 m/Ma (Table 3), yielding to maximum exposure durations ranging between 10.2 and 11.7 ka. Therefore, a maximum abandonment age for the alluvial fan surface of 10–12 ka is retained. Considering an age of ~2 ka for the 1.20 m thick historical colluviums and a maximum abandonment age for the alluvial fan surface of 10–12 ka, this leads to a maximum alluvial fan aggradation duration of 12–14 ka, i.e., approximately coeval with the transition between the Marine Isotopic Stages 2 and 1. This suggests that the fan aggraded at most, after the Last Glacial Maximum, close to the beginning of Holocene.

Finally, as alluvial fan aggradation and abandonment predate the inception of gully incision, it can thus only be concluded that incision started at most 12–14 ka ago. Because only a maximum age for the fan incision can be

Fig. 14 Selected left-lateral offset stream to perform CRE dating and location of the sampling site. **a** Local geological map (close-up of Fig. 5) showing the catchment area of the selected offset stream. **b** Satellite image of the offset stream (same as Fig. 8c, see Fig. 5 for location). Measured offset stream is 54 ± 4 m (50-m minimum considering near-field piercing points, see Suppl. Material Fig. S2). P: sampling site of depth profiles for CRE dating (Fig. 15). **c** Field photograph (looking SW) of the analyzed offset stream. The *green* almond shaped patch facing the upstream gorge corresponds to a shutter ridge. *Purple* wooded area in the background corresponds to the Triassic breccias bedrock of the KSF escarpment; in the foreground, green color corresponds to alluvial fan material and slope screes aggraded on the hanging-wall block
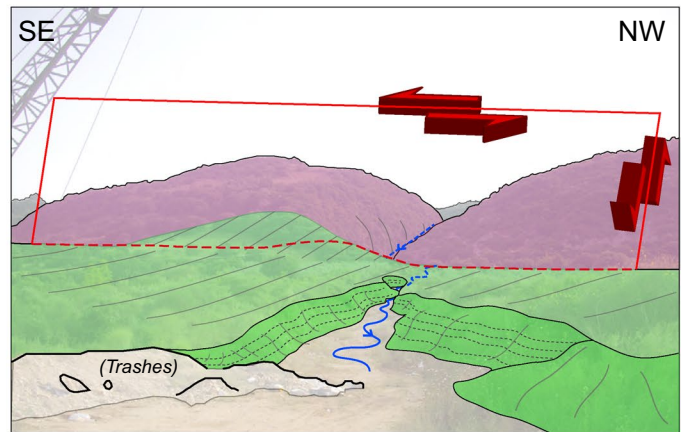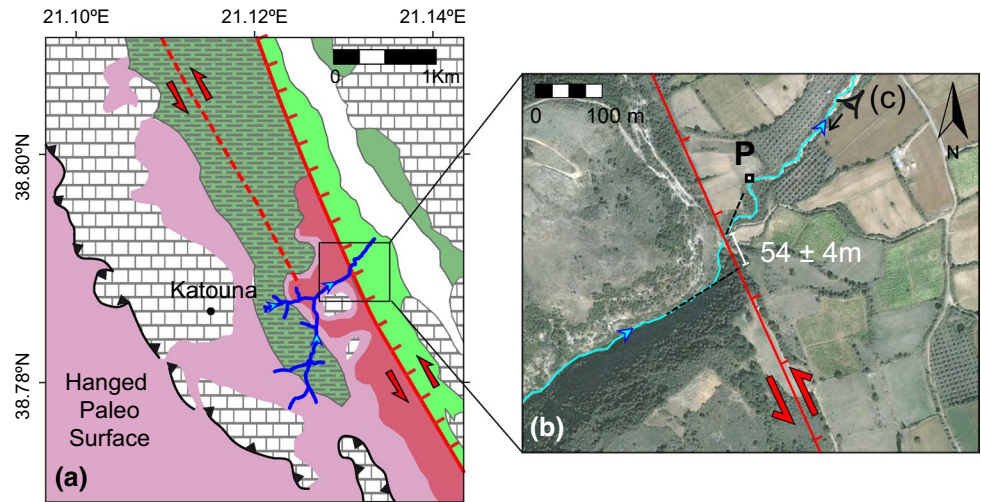
determined, only the minimum slip rate of the KSF can be estimated, using the minimum value of the left-lateral offset. The stream incision offset of at least 50 m (Fig. 14b) that started at most 12–14 ka ago yields an estimated Holocene minimum left-lateral slip rate bracketed between 3.6 and 4.2 mm year^{-1} (~4 mm year^{-1}).

Active kinematics of Western Greece from GPS data

We used the GPS data compilation of Perouse et al. (2012) and added new data. Original GPS vectors (Hollenstein et al. 2008; Floyd et al. 2010; GPSscope permanent GPS

Fig. 15 Sampling site of depth profiles used for CRE dating (located as P on Fig. 14b). Geographic coordinates: 38.79077°N, 21.13115°E. Profile altitude: 95 m. No significant shielding affects the fan surface (maximal values ~10 %). (1) Historic colluviums with heterometric clasts and anthropic elements (tiles, bricks, pottery sherds); (2) Alluvial fan material with heterometric carbonates and cherts clasts within a sandy matrix; PS: pebbly layer; MS: muddy layer with sparse and small angular clasts within a silty-clayed matrix; (3) Alluvial fan material with fairly homometric carbonates and cherts clasts within a sandy matrix
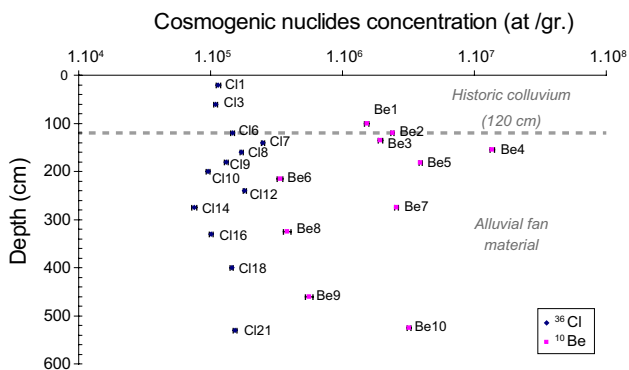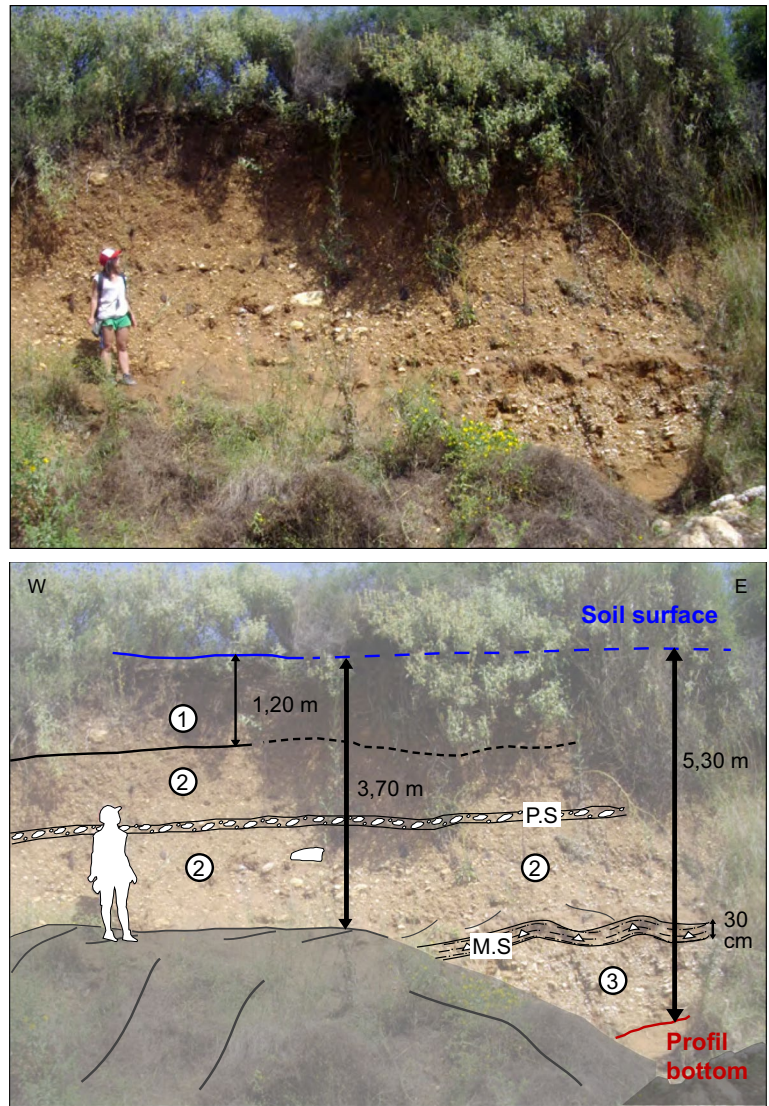

Fig. 16 Measured ^{36}Cl and ^{10}Be concentrations as a function of depth (values in Table 1 and Suppl. Material, Table S1). ^{36}Cl and ^{10}Be have been measured in carbonates and cherts, respectively. This plot emphasizes two distinct origins and pre-exposure histories for carbonates and cherts

network) and new data (Briole 2013) have been rotated into a self-consistent Eurasian reference frame.

GPS velocities in Akarnania can be minimized by a single rigid rotation defining an Akarnania fixed reference frame (Fig. 18). The absence of a gradient in the fault-parallel component of velocity vectors across the KSF attests to localized deformation implying either low elastic coupling (i.e., superficial elastic locking depth) or/and creeping behavior. However, residuals exist in the Ionian Islands. These trend parallel to the Kefalonia fault, and are NE-directed (Fig. 18). To account for this measured GPS velocity field, we interpret the Ionian Islands and Akarnania as moving as a single rigid block: the IAB (Ionian Islands-Akarnania Block). Then, the NE-directed residuals in the Ionian Islands would result from interseismic elastic loading along the dextral Kefalonia fault.
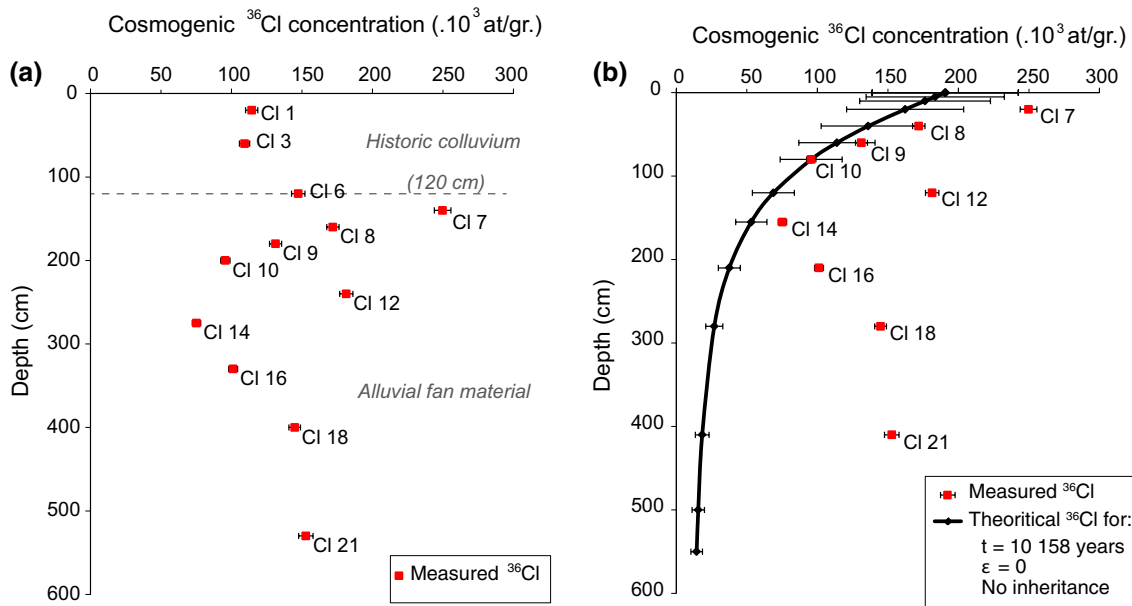
Fig. 17 **a** Measured ^{36}Cl concentrations in carbonate clasts as a function of depth; **b** Rejuvenation depth profile procedure model of ^{36}Cl concentrations (See text for more details). We only consider samples from the alluvial fan material (historic colluviums are not considered, so that the 1.20 m depth corresponds to the initial fan surface). t, maximum in situ exposure duration; ε, denudation rate. The best fit is obtained for zero denudation and Cl 10 sample with a measured ^{36}Cl concentration carrying zero inheritance (Table 2). For all the other samples, the differences between the measured and the modeled concentrations result from pre-exposure processes

Table 1 Measured cosmogenic ^{36}Cl and natural ^{35}Cl concentrations of samples collected along the depth profile at the sampling site (Fig. 15)

Sample	Depth (cm)	Measured ^{36}Cl (at/gr.)	Error measured ^{36}Cl ($\pm$ at/gr.)	Natural 35Cl (ppm)	Geologic material
Cl 01	20	114 310	4 290	25.55	Historic colluviums
Cl 03	60	109 270	3 614	15.93	
Cl 06	120	147 333	4 754	29.10	
Cl 07	140	249 731	5 883	6.89	Alluvial fan
Cl 08	160	171 920	4 357	4.06	
Cl 09	180	131 278	4 247	11.12	
Cl 10	200	95 645	3 297	11.01	
Cl 12	240	181 391	4 702	12.83	
Cl 14	275	75 182	2 964	1.23	
Cl 16	330	101 152	3 130	15.82	
Cl 18	400	144 827	4 134	6.04	
Cl 21	530	152 744	5 144	8.77	

The northern and northeastern boundaries of the IAB would be the Amvrakikos Gulf and the Katouna valley fault (northern KSF), respectively, (Fig. 19). According to GPS vectors on Fig. 18, these structures accommodate IAB/continental Greece relative motion as ~10 mm year^{-1} of N–S extension across the Amvrakikos Gulf and approximately the same amount of left-lateral motion along the Katouna fault, a result in agreement with the Vassilakis et al. (2011) estimation. The actual motion along the Katouna fault (northern KSF) is transtensional: ~11 mm year^{-1} of fault-parallel left-lateral motion and ~3 mm year^{-1} of fault perpendicular extension (Fig. 19). The western boundary of the IAB, which accommodates the relative motion between IAB and the Apulian platform, is the dextral Kefalonia fault. Determining the Kefalonia Fault slip rate is not straightforward as no GPS vectors are available west of the fault, which is an offshore domain (Fig. 18). However, the triple junction occurrence between the Apulian platform, the Continental Greece, and the IAB (Fig. 19) enables a slip rate assessment for the Kefalonia fault: as the

Table 2 Measured ^{36}Cl concentrations and results of depth profile rejuvenation (Fig. 17b)

Sample	Depth (cm)	Nmeas: Measured ^{36}Cl (at/gr.)	Error Nmeas (±at/gr.)	Nth: Theoretical ^{36}Cl for modeled age of 10.158 ka (at/gr.)	Error Nth (at/gr.)	Excess concentration (=Nmeas-Nth) (at/gr.)
Cl 07	20	249 731	5 883	164 721	47 657	85 009
Cl 08	40	171 920	4 357	137 440	38 296	34 480
Cl 09	60	131 278	4 247	114 464	30 875	16 814
Cl 10	80	95 645	3 297	95 645	25 004	0
Cl 12	120	181 391	4 702	68 085	16 749	113 306
Cl 14	155	75 182	2 964	51 971	12 240	23 211
Cl 16	210	101 152	3 130	36 091	8 319	65 061
Cl 18	280	144 827	4 134	25 281	6 239	119 545
Cl 21	410	152 744	5 144	16 810	4 922	135 934

^{36}Cl half-life is 301 ka (Gosse and Phillips 2001). Scaling factor for surface nucleonic and muonic production as a function of latitude and altitude are, respectively, 1.01 and 0.97 (Stone et al. 1996) and have been calculated using CosmoCalc (Vermeesch 2007). We input a bulk rock density of 1.8. Production ^{36}Cl rates and modeling results have been obtained using Excel spreadsheet of (Schimmelpfennig et al. 2009). Spallation production rate from Ca is ~ 42 atoms ^{36}Cl.g.Ca^{-1} (Braucher et al. 2011; Schimmelpfennig et al. 2011). We considered no denudation

Table 3 Maximum modeled ages obtained by depth profile rejuvenation considering different denudation rate values (ε)

Denudation rate ε (m/Ma)	Maximum modeled age (year)
0	10 157.9
5	10 387.2
20	11 155.4
30	11 746.3

Apulian platform converges toward continental Greece at ~5 mm year^{-1} (e.g., Perouse et al. 2012), and considering ~10 mm year^{-1} of N–S extension between IAB and continental Greece, it would imply a Kefalonia fault slip rate of ~15 mm year^{-1} (Fig. 19). Precision of this estimation, which gives an order of magnitude for the Kefalonia fault slip rate, has to be improved in the future accounting elastic coupling processes.

Finally, the Southern Trichonis region belongs neither to continental Greece, nor to the IAB in contrast to what has previously been proposed (Vassilakis et al. 2011). Indeed, this region moves at ~6 mm year^{-1} toward the NW relative to the IAB (Fig. 18). This motion is accommodated by ~6 mm year^{-1} of pure left-lateral strike–slip along the Stamna fault (southern KSF), and ~4 mm year^{-1} of N-S extension across the Trichonis graben (Figs. 18, 19). The Trichonis graben is located at the junction between the northern KSF (Katouna area) and the southern KSF (Stamna area). The ~4 mm year^{-1} of N-S extension across the Trichonis graben would thus account for the left-lateral slip rate difference between the Katouna segment (~11 mm year^{-1} of left-lateral motion) and the Stamna segment (~6 mm year^{-1}). Motions in southern Trichonis increase eastward, reaching values close to those

of continental Greece, resulting in insignificant relative motion between the eastern tip of the southern Trichonis and the western Gulf of Corinth (Fig. 18).

Discussion

A creeping behavior for the KSF?

High slip rate on the KSF (>4 mm year^{-1} according to geological data, possibly up to 11 mm year^{-1} according to GPS) contrasts with the subdued morphological evidence for tectonic activity (this study) and the relatively low level of historical (Papazachos and Papazachou 1997) and instrumental seismicity (Fig. 2). Indeed, if mesoscale deformation is well expressed along the KSF (fault valley, rectilinear convex-shaped upward escarpments, en-échelon fault pattern), the small-scale deformation is nearly missing. The fault shows no clear "earthquake-related" scarps, and scarce well developed dogleg stream offsets. This could suggest that the short-term tectonic landscape is not preserved due to the high level of anthropogenic activity along the KSF. Nevertheless, a strike–slip behavior on a fast slipping KSF should preserve at least some earthquake-related landforms even with high anthropogenic activity. An entirely locked, 11 mm year^{-1}-slipping fault (see previous section) would produce a ~M_w 7 earthquake in average at least each 500 years with a 1–2 m-high scarp, resulting from the expected 3 mm year^{-1} of extension across the northern KSF. Such a scenario is very unlikely, because such a scarp would not be entirely erased everywhere in some hundreds of years and further, there should be some evidence of large earthquakes in the historical

Fig. 18 GPS velocity field relative to fixed Akarnania. GPS sites minimized to define this reference frame are shown with green squares. *Green* diamond site, not used to define the reference frame, shows nonetheless a residual close to zero (See text for discussion). GPS vectors are shown with their 95 % confidence ellipses. Velocity vectors are taken from Hollenstein et al. (2008), Floyd et al. (2010), Briole (2013) and GPSscope data, available at http://crlab.eu
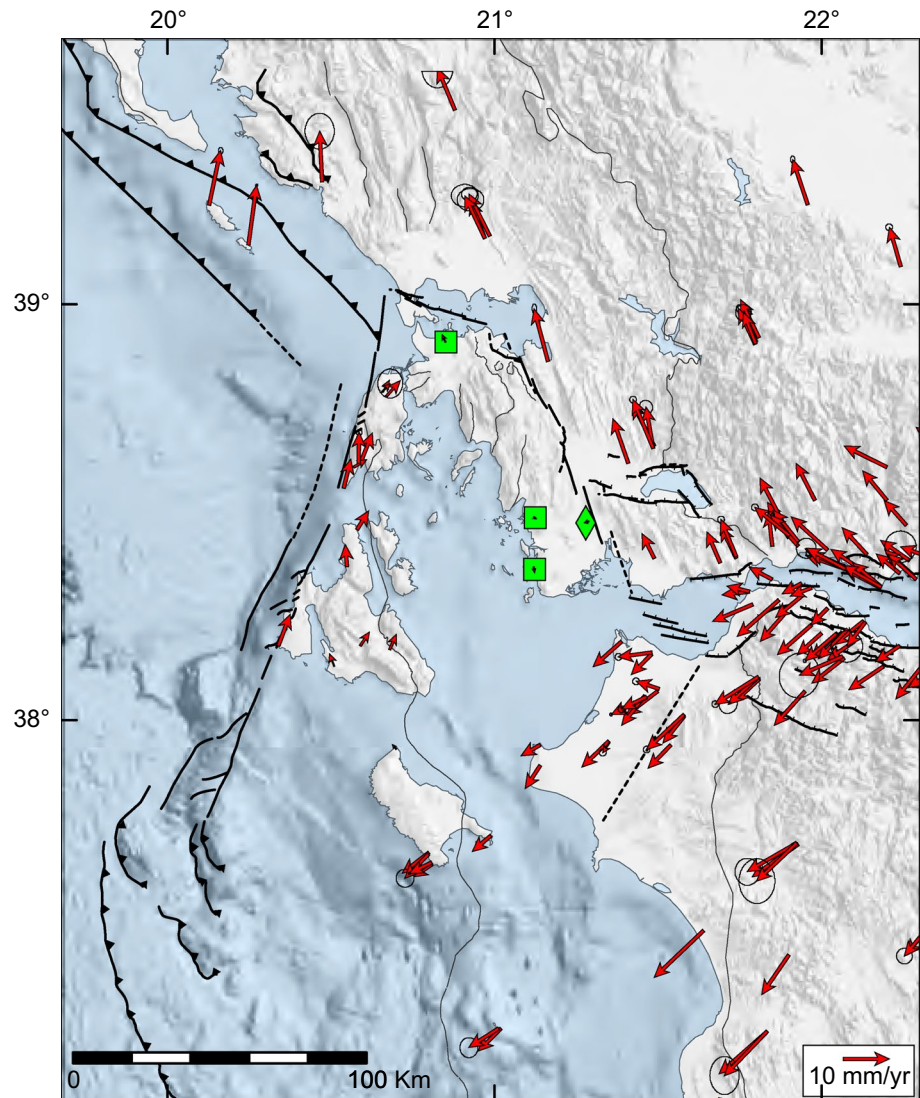

seismicity records. Even assuming that a high percentage of the GPS-derived deformation is transitory and that the average KSF slip rate is closer to the geological minimum estimate, it would not change significantly these conclusions. Consequently, a high percentage of the fault displacement should be accommodated by creep slip. This creep should increase significantly the average return period between two subsequent seismic events as well as lower their magnitudes. Less frequent earthquakes with smaller surface displacements may explain why the small-scale seismic landform is not preserved. Creeping, which may be favored by the gypsum-breccias of the KSF bedrock, is further suggested by the absence of gradient in the fault-parallel component of velocity GPS vectors across the KSF (Fig. 18). It also agrees with the large deficit of seismic moment rate compared to geodetic moment rate in Akarnania (Chousianitis et al. 2015).

Ionian Islands-Akarnania Block (IAB) geometry and kinematics

East of the Kefalonia fault that connects the Apulian collision front to the Hellenic subduction front, we show that deformation in the overriding plate domain is localized along the KSF and the Amvrakikos gulf as no significant deformation occurs along the Neogene N-striking thrusts of Akarnania, located west of the KSF. It delineates a Ionian-Akarnania block (IAB, Fig. 19).

The NNW-striking KSF, northeast boundary of the IAB, terminates northward onto the ESE-striking Loutraki fault. Regionally, the Loutraki fault could belong to an ESE-striking Amvrakikos Gulf half-graben system, with a northward dipping master fault (Fig. 3). Indeed, E–W active fault segments have been imaged at the western termination of the Gulf (sparker seismic reflection profiles, Anastasakis et al. 2007). The submerged morphology, the southward

Fig. 19 Simplified tectonic map of Western Greece. IAB: Ionian Islands-Akarnania Block. *Arrows* and *numbers* show relative motions and fault slip rate values in mm/year. *Italic numbers* refer to GPS slip rate determined in previous studies (Briole et al. 2000; Perouse et al. 2012). *Regular numbers* indicate GPS slip rate assessed in this study. The minimum geological slip rate determined from CRE dating for the Katouna fault is reported as (geol). *Dotted* areas are diffused deformation zones. Green asterisk and dashed line point to possible incipient fault (see "Discussion" for details)
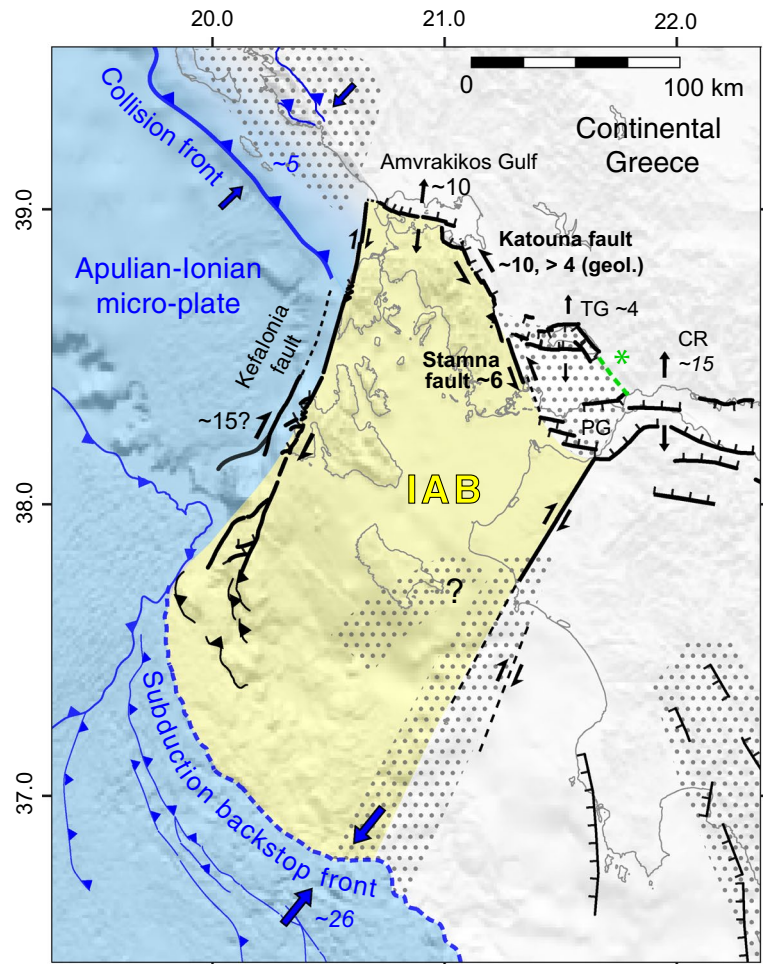
flexure and the absence of clear E-W active normal fault trace on the northern side of the Amvrakikos Gulf suggest a half-graben geometry. However, the eastern submerged part of the Gulf has not been imaged yet, so we cannot clearly constrain what is controlling the subsidence east the Loutraki fault. The ESE-striking Amvrakikos Gulf half-graben system we propose would represent the northern boundary of the IAB. The western and southwestern boundaries of the IAB would be the Kefalonia fault and the Hellenic subduction front, respectively (Fig. 19). Finally, the IAB southeastern boundary might be located in the NW Peloponnesus, along the right-lateral Achaia-Elia fault (Fig. 19) associated with the 2008 M_w 6.4 Movri earthquake (Serpetsidaki et al. 2014). This Achaia-Elia fault zone should accommodate the relative motion between the IAB and the Peloponnesus. The trenchward motions of these two blocks are ~10 mm/year for the IAB (constrained by the KSF rate) and some ~15 mm/year for the Peloponnesus (constrained by the opening rate of the Corinth Rift), respectively. Consequently the right-lateral rate of the Achaia-Elia fault zone should be ~ 5 mm/yr. In our model, the Gulf of Patras graben system should correspond to a triple junction

between the western tip of the Corinth Rift, the KSF, and the Achaia-Elia Fault zone (Fig. 19). In more details, the triple junction zone between Peloponnesus, Continental Greece, and our determined IAB could actually be a diffuse zone spread over the Nafpaktos basin (basin linking the western tip of the Corinth rift to the Patras gulf), as proposed by Beckers et al. (2015), based on a submarine active faults study of the region. Thus, kinematics of the IAB fault boundaries indicates a trenchward motion, compatible with the regional Hellenic slab retreat.

At first order, the IAB geometry we propose in this paper shares several similarities with the Akarnania "fragment" proposed by Vassilakis et al. (2011). However, our study delineates the NNW-striking Stamna fault segment as the southeastern prolongation of the Katouna fault, indicating the southern KSF fault system connects directly with the Patras Gulf, contrasting with a Amphilochia valley–Trichonis graben–Gulf of Corinth faults network (Vassilakis et al. 2011). Consequently, in our model, the opening of the Trichonis graben, located at the junction between the Katouna and the Stamna faults, accommodates the left-lateral slip rate difference between the northern and southern

KSF (Figs. 18, 19). Finally, despite a high seismic activity along a NW trend connecting the western tip of the Corinth rift to the Trichonis graben (Fig. 2, Evangelidis et al. 2008; Kiratzi et al. 2008), active faulting is not observed either in the morphology or from GPS data (Fig. 18). It suggests that this area, seismically "crackling," could represent an incipient fault zone, not yet established (Fig. 19).

Timing individualization of the Ionian Islands-Akarnania Block (IAB)

Such a high slip rate on short surface fault segments suggests that the KSF (northeastern boundary of the IAB, Fig. 19) is not yet a mature system. The direction of the KSF, collinear with the NNW-striking Ionian thrust formed during Hellenides orogen (Figs. 3, 4), suggests structural inheritance. However, in the Katouna area, our results show that the KSF is a steep fault, crosscutting the Ionian thrust sheet at depth (Fig. 7). The KSF could thus be a neoformed fault, but whose direction has been controlled by the Hellenides orogen fabric.

As the KSF is directly connected to the Loutraki fault, initiation of the Loutraki fault/Amvrakikos half-graben and the KSF should be synchronous. According to the sedimentological record of Amvrakikos Gulf series, regional subsidence in the Amvrakikos Gulf would have initiated at least since MIS 8 (245-300 ka, Anastasakis et al. 2007). In addition, due to the triple junction between Continental Greece, the Apulian-Ionian micro-plate and the IAB (Fig. 19), extension initiation across the Amvrakikos Gulf may be contemporary or younger than dextral initiation along the Kefalonia fault. Dextral shear along the Kefalonia fault, an inherited normal fault of the Apulian platform (Sorel 1976), would have initiated ca. 1.5–1.3 Ma (Sorel 1976; Cushing 1985; Nielsen 2003). The present-day Loutraki fault has an escarpment height of ~700 m (Fig. 6). For comparison, the East Helike fault, a northward dipping active normal fault of the Corinth Rift system having a ~800 m escarpment height (1600 m of total vertical throw, ~800 of footwall uplift, ~800 of hanging-wall subsidence), and which extension rate evolution is well constrained, would have initiated at 700–800 ka (McNeill and Collier 2004; Ford et al. 2013). However, as we have no constrains about the Loutraki fault extension rate evolution, a reasonable age initiation for the Loutraki fault/Amvrakikos Gulf system (and consequently its connected KSF) can thus be bracketed between ~1.5 Ma and 300 ka. Finally, our observations suggest that no more internal E–W compression occurs in Akarnania since ~600 ka since the N-striking Astakos thrust is sealed by Middle Pleistocene slope breccia (Figs. 12, 13). All these age constraints and faults geometries in Akarnania

are compatible with a change from E–W compressional stress regime to a near N–S horizontal σ_3 axis during the Pleistocene, leading to the progressive individualization and trenchward motion of the IAB. Hence, initiation of the IAB individualization could be coeval with the Corinth rifting phase 2 or 3 (~1.7 Ma to ~700 ka, and ~700 ka to present-day, respectively, Ford et al. 2013). The right-lateral Achaia-Elia fault, potential southeastern boundary of the IAB, is considered juvenile because no coseismic surface rupture occurred during the 2008 M_w 6.4 Movri earthquake (Feng et al. 2010) and no morphological evidence attests long-term fault activity (Stiros et al. 2013).

Conclusion

An accurate mapping of active and inactive fault traces, new multi-scale geomorphologic and tectonic observations and a geodetic study provide evidence for active normal and left-lateral faulting along the Katouna-Stamna Fault (KSF), a 65-km-long NNW-striking fault system connecting the Amvrakikos Gulf to the Patras Gulf. The KSF segments are typically ~10 km long. We further show that the N-striking Cenozoic Hellenides thrusts, located west of the KSF in Akarnania, are no longer active, by either field observation or GPS data. It results that the transition from subduction to collision in Western Greece is accommodated in the overriding plate by the individualization of a Ionian Island-Akarnania block (IAB, Fig. 19). The KSF, that we interpret as a neoformed immature fault system, but which strike is likely to be inherited from the Hellenides orogen, forms presently the northeastern boundary of the IAB. The northern KSF accommodates IAB motion relative to continental Greece by active left-lateral transtension along the Katouna valley. The southern KSF accommodates relative motion between the IAB and the southern Trichonis Lake region by left-lateral slip along the Stamna fault. The KSF slip rate is high: at least 4 mm year^{-1} of geological slip rate was determined by CRE dating on the Katouna valley segment. GPS data shows ~11 mm year^{-1} and ~6 mm year^{-1} of left-lateral slip rate along the northern KSF (Katouna segments) and the southern KSF (Stamna segments), respectively. We suggest the localized strain and high slip rate along the KSF should be dominantly released by aseismic creep, compatible with the gypsum-breccias bedrock along the fault and the low level of seismicity. We finally propose that a change from E–W compressional stress regime to a near N–S horizontal σ_3 axis would have occurred in Akarnania during the Pleistocene, leading to the progressive individualization and trenchward motion of the IAB from Pleistocene time (younger than ~1.5 Ma) to present day.

References

Anastasakis G, Piper DJW, Tziavos C (2007) Sedimentological response to neotectonics and sea-level change in a delta-fed, complex graben: Gulf of Amvrakikos, western Greece. Mar Geol 236:27–44. doi:10.1016/j.margeo.2006.09.014

Aubouin J (1959) Contribution à l'étude géologique de la Grèce septrionale; les confins de l'Epire et de la Thessalie. Annales Géologiques des pays Hélleniques 9

Beckers A, Hubert-Ferrari A, Beck C, Bodeux S, Tripsanas E, Sakellariou D, De Batist M (2015) Active faulting at the western tip of the Gulf of Corinth, Greece, from high-resolution seismic data. Mar Geol 360:55–69

Braucher R, Del Castillo P, Siame L, Hidy AJ, Bourles DL (2009) Determination of both exposure time and denudation rate from an in situ-produced Be-10 depth profile: a mathematical proof of uniqueness. Model sensitivity and applications to natural cases. Quat Geochronol 4:56–67. doi:10.1016/j.quageo.2008.06.001

Braucher R, Merchel S, Borgomano J, Bourles DL (2011) Production of cosmogenic radionuclides at great depth: a multi element approach. Earth Planet Sci Lett 309:1–9. doi:10.1016/j.epsl.2011.06.036

Briole P (2013) Ground deformation across the Corinth rift from 22 years of GPS observations. Geophysical Research Abstracts 15:EGU2013-13183, EGU General Assembly, Vienna, Austria

Briole P, Rigo A, Lyon-Caen H, Ruegg JC, Papazissi K, Mitsakaki C, Balodimou A, Veis G, Hatzfeld D, Deschamps A (2000) Active deformation of the Corinth rift, Greece: results from repeated Global Positioning System surveys between 1990 and 1995. J Geophys Res-Solid Earth 105:25605–25625

British Petroleum Co Ltd (1971) The Geological Results of Petroleum Exploration in Western Greece. Institute of Geology and Mineral Exploration, IGME, Special Report, 10, Athens

Catalano R, Doglioni C, Merlini S (2001) On the Mesozoic Ionian Basin. Geophys J Int 144:49–64. doi:10.1046/j.0956-540X.2000.01287.x

Chamot-Rooke N, Rangin C, Le Pichon X, Dotmed working group (2005) DOTMED: a synthesis of deep marine data in the eastern Mediterranean. Mém Soc Géol France 177:64p

Chousianitis K, Ganas A, Evangelidis CP (2015) Strain and rotation rate patterns of mainland Greece from continuous GPS data and comparison between seismic and geodetic moment release. J Geophys Res: Solid Earth. doi:10.1002/2014JB011762

Clews JE (1989) Structural controls on basin evolution: Neogene to Quaternary of the Ionian zone, Western Greece. J Geol Soc Lond 146:447–457

Cocard M, Kahle HG, Peter Y, Geiger A, Veis G, Felekis S, Paradissis D, Billiris H (1999) New constraints on the rapid crustal motion of the Aegean region: recent results inferred from GPS measurements (1993–1998) across the West Hellenic Arc, Greece. Earth Planet Sci Lett 172:39–47

Collier REL, Dart CJ (1991) Neogene to Quaternary rifting, sedimentation and uplift in the Corinth Basin, Greece. J Geol Soc Lond 148:1049–1065

Cushing M (1985) Evolution structurale de la marge nord ouest Héllenique dans l'île de Levkas et ses environs (Grèce nord-occidentale). Université Paris-Sud (XI), Centre d'Orsay, France

D'Agostino N, Avallone A, Cheloni D, D'Anastasio E, Mantenuto S, Selvaggi G (2008) Active tectonics of the Adriatic region from GPS and earthquake slip vectors. J Geophys Res-Solid Earth 113:B12413. doi:10.1029/2008JB005860

Durand V, Bouchon M, Floyd MA, Theodulidis N, Marsan D, Karabulut H, Schmittbuhl J (2014) Observation of the spread of slow deformation in Greece following the breakup of the slab. Geophys Res Lett 41:7129–7134

Engdahl ER, van der Hilst R, Buland R (1998) Global teleseismic earthquake relocation with improved travel times and procedures for depth determination. Bull Seismol Soc Am 88:722–743

Evangelidis CP, Konstantinou KI, Melis NS, Charalambakis M, Stavrakakis GN (2008) Waveform relocation and focal mechanism analysis of an earthquake swarm in Trichonis Lake, western Greece. Bull Seismol Soc Am 98:804–811

Feng LJ, Newman AV, Farmer GT, Psimoulis P, Stiros SC (2010) Energetic rupture, coseismic and post-seismic response of the 2008 M-W 6.4 Achaia-Elia Earthquake in northwestern Peloponnese, Greece: an indicator of an immature transform fault zone. Geophys J Int 183:103–110. doi:10.1111/j.1365-246X.2010.04747.x

Ferentinos G, Brooks M, Doutsos T (1985) Quaternary tectonics in the Gulf of Patras, Western Greece. J Struct Geol 7:713–717. doi:10.1016/0191-8141(85)90146-4

Floyd MA, Billiris H, Paradissis D, Veis G, Avallone A, Briole P, McClusky S, Nocquet JM, Palamartchouk K, Parsons B, England PC (2010) A new velocity field for Greece: implications for the kinematics and dynamics of the Aegean. J Geophys Res-Solid Earth 115:B10403. doi:10.1029/2009JB007040

Ford M, Rohais S, Williams EA, Bourlange S, Jousselin D, Backert N, Malartre F (2013) Tectono-sedimentary evolution of the western Corinth rift (Central Greece). Basin Res 25:3–25

Gasse F, Vidal L, Van Campo E, Demory F, Develle A-L, Tachikawa K, Elias A, Bard E, Garcia M, Sonzogni C (2015) Hydroclimatic changes in northern Levant over the past 400,000 years. Quat Sci Rev 111:1–8

Gaudemer Y, Tapponier P, Turcotte DL (1989) River offsets across active strike-slip faults. Annales Tectonicae 3:55–76

Gosse JC, Phillips FM (2001) Terrestrial in situ cosmogenic nuclides: theory and application. Quat Sci Rev 20:1475–1560. doi:10.1016/S0277-3791(00)00171-2

GPS scope (permanent GPS network) supervised by Briole P, Charade O, and Ganas, A. On-line data available at http://crlab.eu

Haslinger F, Kissling E, Ansorge J, Hatzfeld D, Papadimitriou E, Karakostas V, Makropoulos K, Kahle HG, Peter Y (1999) 3D crustal structure from local earthquake tomography around the Gulf of Arta (Ionian region, NW Greece). Tectonophysics 304:201–218. doi:10.1016/S0040-1951(98)00298-4

Hatzfeld D, Kassaras I, Panagiotopoulos D, Amorese D, Makropoulos K, Karakaisis G, Coutant O (1995) Microseismicity and strain pattern in northwestern Greece. Tectonics 14:773–785

Hollenstein C, Muller MD, Geiger A, Kahle HG (2008) Crustal motion and deformation in Greece from a decade of GPS measurements, 1993–2003. Tectonophysics 449:17–40

Institute of Geology and Mineral Exploration (IGME) (1987) Geological map of Greece, Amphilochia sheet, 1:50 000

Jolivet L, Labrousse L, Agard P, Lacombe O, Bailly V, Lecomte E, Mouthereau F, Mehl C (2010) Rifting and shallow-dipping detachments, clues from the Corinth Rift and the Aegean. Tectonophysics 483:287–304. doi:10.1016/j.tecto.2009.11.001

Karakitsios V, Rigakis N (2007) Evolution and petroleum potential of Western Greece. J Petrol Geol 30:197–218. doi:10.1111/j.1747-5457.2007.00197.x

Kiratzi A, Sokos E, Ganas A, Tselentis A, Benetatos C, Roumelioti Z, Serpetsidaki A, Andriopoulos G, Galanis O, Petrou P (2008) The April 2007 earthquake swarm near Lake Trichonis and implications for active tectonics in western Greece. Tectonophysics 452:51–65. doi:10.1016/j.tecto.2008.02.009

Konstantinou KI, Melis NS, Lee SJ, Evangelidis CP, Boukouras K (2009) Rupture Process and Aftershocks Relocation of the 8 June 2008 M-w 6.4 Earthquake in Northwest Peloponnese, Western Greece. B Seismol Soc Am 99:3374–3389. doi:10.1785/0120080301

Le Dortz K, Meyer B, Sebrier M, Braucher R, Bourles D, Benedetti L, Nazari H, Foroutan M (2012) Interpreting scattered in situ produced cosmogenic nuclide depth-profile data. Quat Geochronol 11:98–115. doi:10.1016/j.quageo.2012.02.020

Le Pichon X, Chamot-Rooke N, Lallemant S, Noomen R, Veis G (1995) Geodetic determination of the kinematics of central Greece with respect to Europe: implications for eastern Mediterranean tectonics. J Geophys Res 100:12675–12690. doi:10.1029/95jb03170

Louvari E, Kiratzi AA, Papazachos BC (1999) The Cephalonia Transform Fault and its extension to western Lefkada Island (Greece). Tectonophysics 308:223–236

McNeill LC, Collier REL (2004) Uplift and slip rates of the eastern Eliki fault segment, Gulf of Corinth, Greece, inferred from Holocene and Pleistocene terraces. J Geol Soc Lond 161:81–92. doi:10.1144/0016-764903-029

Melis NS, Burton PW (1988) Seismicity and crustal deformation in regions of Central Greece. Geophys J R Astr Soc 92:529

Nielsen C (2003) Etude des zones de subduction en convergence hyper-oblique: exemples de la ride méditerranéenne et de la marge indo-birmane. Université Paris-Sud (XI), Centre d'Orsay, France

Nishiizumi K, Imamura M, Caffee MW, Southon JR, Finkel RC, McAninch J (2007) Absolute calibration of Be-10 AMS standards. Nucl Instrum Meth B 258:403–413. doi:10.1016/j.nimb.2007.01.297

Papanikolaou D, Alexandri M, Nomikou P (2006) Active faulting in the north Aegean basin. Geol S Am S 409:189–209. doi:10.1130/2006.2409(11)

Papazachos B, Papazachou C (1997) The earthquakes of Greece. P. Ziti and Co, Thessaloniki

Pearce FD, Rondenay S, Sachpazi M, Charalampakis M, Royden LH (2012) Seismic investigation of the transition from continental to oceanic subduction along the western Hellenic Subduction Zone. J Geophys Res-Solid Earth. doi:10.1029/2011JB009023

Perouse E (2013) Cinématique et tectonique active de l'Ouest de la Grèce dans le cadre géodynamique de la Méditerranée Centrale et Orientale. Université Orsay - Paris Sud, Paris XI

Perouse E, Chamot-Rooke N, Rabaute A, Briole P, Jouanne F, Georgiev I, Dimitrov D (2012) Bridging onshore and offshore present-day kinematics of central and eastern Mediterranean: implications for crustal dynamics and mantle flow. Geochem Geophy Geosy. doi:10.1029/2012gc004289

Rohais S, Eschard R, Ford M, Guillocheau F, Moretti I (2007a) Stratigraphic architecture of the Plio-Pleistocene infill of the Corinth Rift: implications for its structural evolution. Tectonophysics 440:5–28. doi:10.1016/j.tecto.2006.11.006

Rohais S, Joannin S, Colin J-P, Suc J-P, Guillocheau F, Eschard R (2007b) Age and environmental evolution of the syn-rift fill of the southern coast of the Gulf of Corinth (Akrata-Derveni region, Greece). Bulletin de la Société géologique de France 178:231–243

Schimmelpfennig I, Benedetti L, Finkel R, Pik R, Blard PH, Bourles D, Burnard P, Williams A (2009) Sources of in situ Cl-36 in basaltic rocks. Implications for calibration of production rates. Quat Geochronol 4:441–461. doi:10.1016/j.quageo.2009.06.003

Schimmelpfennig I, Benedetti L, Garreta V, Pik R, Blard PH, Burnard P, Bourles D, Finkel R, Ammon K, Dunai T (2011) Calibration of cosmogenic Cl-36 production rates from Ca and K spallation in lava flows from Mt. Etna (38 degrees N, Italy) and Payun Matru (36 degrees S, Argentina). Geochim Cosmochim Ac 75:2611–2632. doi:10.1016/j.gca.2011.02.013

Serpetsidaki A, Elias P, Ilieva M, Bernard P, Briole P, Deschamps A, Lambotte S, Lyon-Caen H, Sokos E, Tselentis G-A (2014) New constraints from seismology and geodesy on the Mw = 6.4 2008 Movri (Greece) earthquake: evidence for a growing strike-slip fault system. Geophys J Int 198:1373–1386

Siame L, Bellier O, Braucher R, Sebrier M, Cushing M, Bourles D, Hamelin B, Baroux E, de Voogd B, Raisbeck G, Yiou F (2004) Local erosion rates versus active tectonics: cosmic ray exposure modelling in Provence (south-east France). Earth Planet Sci Lett 220:345–364. doi:10.1016/S0012-821x(04)00061-5

Sorel D (1976) Etude néotectonique dans l'arc Egéen externe occidental: les îles Ioniennes de Céphalonie et Zanthe et de l'Elide occidentale (Grèce). Université Paris-Sud (XI), Centre d'Orsay, France

Sorel D (1989) L'évolution structurale de la Grèce nord-occidentale depuis le Miocène, dans le cadre géodynamique de l'arc égéen. Université Paris-Sud (XI), Centre d'Orsay, France

Speranza F, Minelli L, Pignatelli A, Chiappini M (2012) The Ionian Sea: the oldest in situ ocean fragment of the world? J Geophys Res-Solid Earth. doi:10.1029/2012jb009475

Stiros S, Moschas F, Feng LJ, Newman A (2013) Long-term versus short-term deformation of the meizoseismal area of the 2008 Achaia-Elia (M-W 6.4) earthquake in NW Peloponnese, Greece: evidence from historical triangulation and morphotectonic data. Tectonophysics 592:150–158. doi:10.1016/j.tecto.2013.02.016

Stone JO, Allan GL, Fifield LK, Cresswell RG (1996) Cosmogenic chlorine-36 from calcium spallation. Geochim Cosmochim Acta 60:679–692. doi:10.1016/0016-7037(95)00429-7

Underhill JR (1989) Late Cenozoic deformation of the Hellenide foreland, western Greece. Geol Soc Am Bull 101:613–634

Vassilakis E, Royden L, Papanikolaou D (2006) Extensional neotectonic structures adjacent and sub-parallel to the Hellenic trench. GSA Abstracts with Programs, Vol 38/7, Philadelphia

Vassilakis E, Royden L, Papanikolaou D (2011) Kinematic links between subduction along the Hellenic trench and extension in the Gulf of Corinth, Greece: a multidisciplinary analysis. Earth Planet Sci Lett 303:108–120. doi:10.1016/j.epsl.2010.12.054

Vermeesch P (2007) CosmoCalc: an excel add-in for cosmogenic nuclide calculations. Geochem Geophy Geosy. doi:10.1029/2006gc001530

Wallace RE (1978) Geometry and rates of change of fault-generated range fronts, north-central Nevada. J Res US Geol Surv 6:637–649

Zerathe S, Braucher R, Lebourg T, Bourles D, Manetti M, Leanni L (2013) Dating chert (diagenetic silica) using in situ produced Be-10: possible complications revealed through a comparison with Cl-36 applied to coexisting limestone. Quat Geochronol 17:81–93. doi:10.1016/j.quageo.2013.01.003